2022

The Role of IRF-1 in Spontaneous Mouse Glioma

Aakash B. Vaidya
Virginia Commonwealth University

THE ROLE OF IRF-1 IN SPONTANEOUS MOUSE GLIOMA

A thesis submitted in partial fulfillment of the requirements for the degree of Biochemistry at Virginia Commonwealth University.

by

AAKASH VAIDYA
Bachelor of Science in Finance and Marketing, University of Colorado Boulder, 2018

Director: TOMASZ KORDULA
PROFESSOR, DEPARTMENT OF BIOCHEMISTRY AND MOLECULAR BIOLOGY

Virginia Commonwealth University
Richmond, Virginia
May, 2022

ACKNOWLEDGEMENTs

I would like to start with a Sanskrit phrase; Gurur Brahma Gurur Vishnu, Gurur Devo Maheshwarah, Guru Saakshaata Parabrahma, Tasmai Shri Guruve Namah. This is what we say in Sanskrit to thank our mentors for guiding us on the path of knowledge. I am very thankful to my mentor, Dr. Tomasz Kordula. He took me into his lab after the completion of my Health Sciences Certificate program and found a way to incorporate me into his research protocol with ease. Even though I had taken a year off from school and had never worked in such a rigorous lab, he guided me through the process.

I would also like to thank Alexandra Krebs Gonsiewski and Karli Mockenhaupt for helping to teach me all the different lab protocols. They took considerable amounts of time to ensure I knew all the processes to be able to complete my research accordingly. In that same breath, I would like to thank Alexandra yet again for helping me by capturing such stunning confocal images. Without her, I would not have been to properly gather all my data.

I would also like to thank my committee members, Dr. Sandeep Singh and Dr. Kristoffer Valerie for being so open to accepting my thesis and timeline. It has been a marathon to get it all completed and so I greatly appreciate their patience.

Finally, I would like to thank all the loved ones in my life especially my parents Dr. Bharat Vaidya and Anupama Vaidya. They have always supported me in my pursuits and continue to do so as I look to medical school in the future.

Table of Contents

List of Figures

Page

ABSTRACT

THE ROLE OF IRF-1 IN SPONTANEOUS MOUSE GLIOMA

By Aakash B Vaidya

A Thesis submitted in partial fulfillment of the requirements for the degree of Masters of Biochemistry at Virginia Commonwealth University.

Virginia Commonwealth University, 2022

Major Director: Dr. Tomasz Kordula

Professor, Department of Biochemistry

Glioblastoma Multiforme has been shown to be one of the deadliest primary brain cancers. One of the reasons why GBM is so deadly, is a unique immunosuppressive tumor microenvironment that promotes GBM growth and progression. Both astrocyte and microglia have been implicated in immunosuppression. In this study, we explored the role of Interferon Regulatory Factor 1 (IRF-1) in astrocytes and glioma cells on the growth of spontaneous glioma tumors. IRF-1 is regulated by the JAK/STAT pathway and induces expression of Programmed death ligand 1 (PD-L1). PD-L1 downregulates immune responses to glioma. We found that IRF-1 had no effect on spontaneous glioma generation nor growth. We also discovered that PD-L1 expression was downregulated in glioma cells. There was still high PD-L1 expression in microglia. Interestingly, we found that tumor

vascularization was significantly decreased in animals lacking IRF-1 expression in astrocytes. This has been associated with the loss of CD31 positive staining in endothelial cells as well as the loss of AQP4 expression. Our data suggests that astrocytic IRF-1 may control tumor vascularization via regulating astrocytic endfeet.

CHAPTER 1

INTRODUCTION

Glioblastoma-Multiforme (GBM) is one of the deadliest forms of primary tumors. They are the most commonly occurring primary brain tumors within the central nervous system. GBM accounts for over 60% of all primary brain tumors in adults (Hanif et al,. 2017). The lifespan of someone with GBM is 12-18 months after diagnosis if lucky. Only 25% of patients make it past one year with the tumor, and 5% make it past 5 years (Hanif et al,. 2017). Current treatment for GBM is tumor removal surgery followed by daily radiation and an oral chemotherapy regimen (Wang et al,. 2021). However, this does not remove all the tumor cells and the tumor continues to proliferate. Despite all the forms of modern immunotherapies that are used in cancer treatment, GBM remains very elusive and impossible to fully treat.

There are many risk factors associated with GBM. Some of the main reasons seem to be genetic disorders, such as neurofibromatosis, environmental factors, such as pesticides, and other reasons that may not fit into a specific category (Hanif et al,. 2017).

GBM is encapsulated by a microenvironment that is highly immunosuppressive, which leads to rapid malignancy as well as its resistance to common immunotherapies that we employ for other forms of cancer (Pombo Antunes et al,. 2020). This microenvironment is constituted of tumor associated macrophages, tumor-infiltrating dendritic cells, regulatory T-Cells, monocytes, microglia, and tumor-associated astrocytes (Figure 1). This immunosuppressive tumor microenvironment tones down the immune system response. The microenvironment uses different signaling pathways to suppress cytotoxic anti-tumor T-Cell response to the tumor. This allows for the tumor to evade the body's immune system and continue to grow unchecked (Pombo Antunes et al,. 2020).

Research about this tumor microenvironment continues to give us greater insight into how it functions. Recently, it has been shown that the JAK-STAT pathway is activated in astrocytes within the tumor microenvironment (Zhang et al,. 2020). Research has also shown that crosstalk between astrocytes lining the outside of the tumor and the microglia that infiltrate the inside of the tumor microenvironment help to induce the immunosuppressive state associated with GBMs (Pombo Antunes et al,. 2020).

To further investigate GBMs and the reasoning behind their immunosuppressive nature, there needs to be greater focus on the immune responses that occurs during tumorigenesis, the downstream effects, and the reason why that response may get shunted.

Figure 1: Glioblastoma Associated Microenvironment. These are some of the cells that make up the tumor microenvironment. These cells include tumor associated macrophages, tumor associated astrocytes, tumor-infiltrating dendritic cells, regulatory T-Cells, monocytes, and microglia.

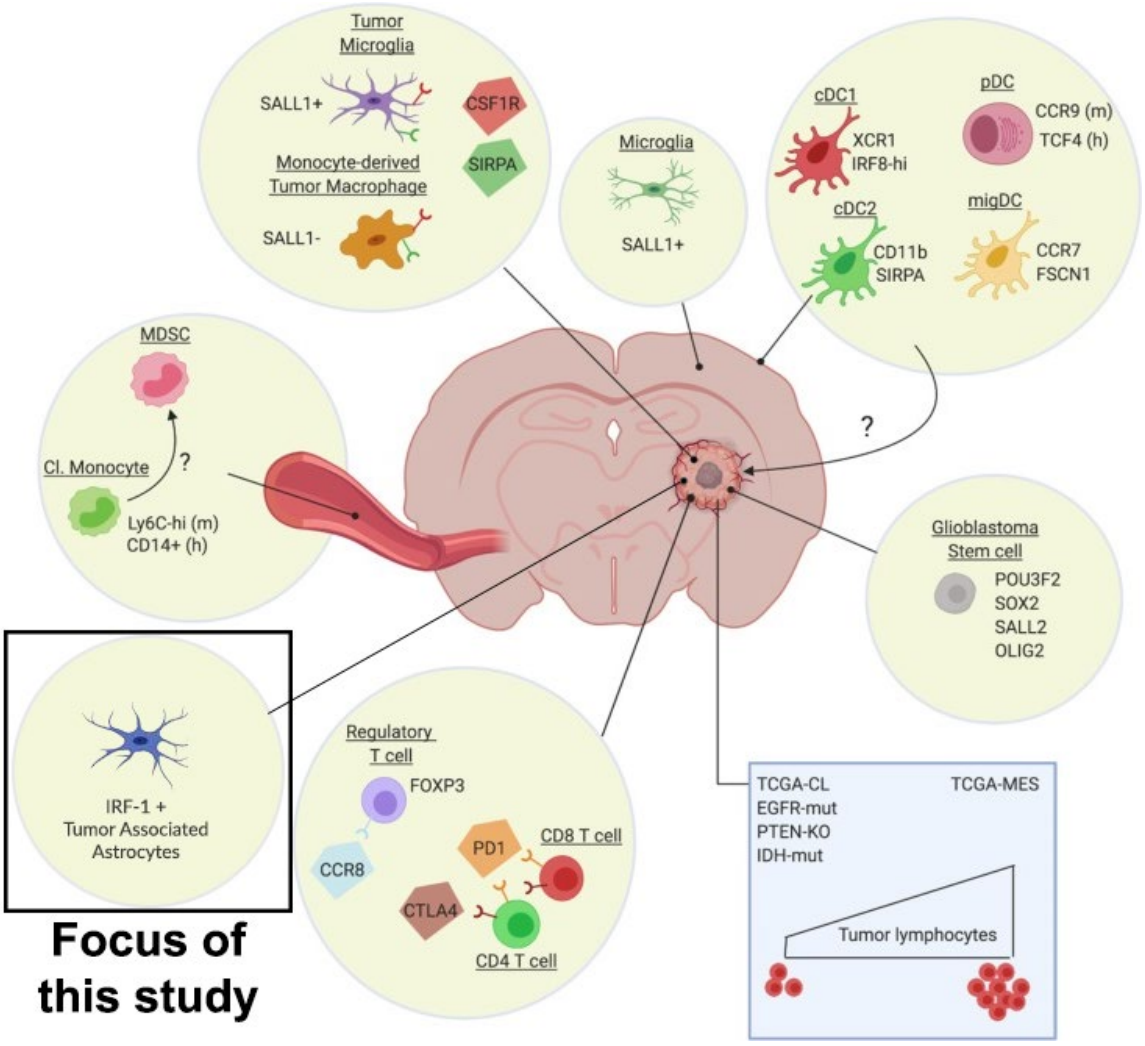

ADOPTED FROM: Pombo Antunes, Ana Rita et al. "Understanding the glioblastoma immune microenvironment as basis for the development of new immunotherapeutic strategies." *eLife* vol. 9 e52176. 4 Feb. 2020, doi:10.7554/eLife.521a76

CD8-Postive T-Cells ($CD8^+$ T-cells) are vital major histocompatibility complex (MHC) class 1-restricted T-cells that mediate adaptive immunity (Figure 1). One population are cytotoxic T-cells, which are critical for anti-tumor immune responses (Iwahori. 2020). After recognition of tumor cells with a T-Cell Receptor (TCR), a CD8+ T-cell secretes different cytokines to regulate anti-tumor immune response, including Interferonγ (IFNγ).

Interferonγ (IFNγ) is a Type II interferon. IFNs were first regarded as substances that affect and downregulates viral replication. It is a form of cytokine that plays a key role in the innate and adaptive immunity. IFNγ is a monomer that consists of a core made up of six α-helices and an unfolded sequence in the C-terminus (Karki et al,. 2021). This structure allows for its receptor binding. It binds a heterodimeric receptors consisting of Interferon Gamma Receptor 1 (IFNGR1) and Interferon Gamma Receptor 2 (IFNGR2) (Karki et al,. 2021).

IFNγ is secreted by activated lymphocytes, such as helper T cells and natural killer cells (NK). It is released in response to viral or bacterial infection, immunoregulation, and tumorigenesis. Its production and subsequent release are regulated by other cytokines, including interleukin-12 (IL-12) and IL-18, which are secreted by other cells such as macrophages (Schroder et al., 2004). IFNγ plays a key role in transcriptional regulation of many downstream genes via the JAK-STAT pathway (Garcia-Diaz et al,. 2017).

JAK-STAT Pathway is one of the key pathways that is essential for transcription regulation in response to Interferonγ (IFNγ). The Janus Tyrosine Kinase (JAK) family consists of JAK1, JAK2, JAK3, and Tyk2 (Imada et al., 2000). JAKs are tyrosine kinases with seven conserved JH regions. The JH1 is the functional catalytic domain and the JH2 region being the pseudokinase domain (Imada et al., 2000).

Genes encoding Signal Transducer and Activator of Transcription (STAT) proteins are localized as clusters on chromosomes, with STAT 1 and 4 on human chromosome 1, STAT 2 and 6 on chromosome 1-, and STAT 3, 5a, and 5b on chromosome 11 (Harrison et al,. 2012). All STATS contain an SH2 domain that is essential for the process of dimerization and receptor binding. All STATs contain a tyrosine residue approximately 700 residues from the N-Terminus that is phosphorylated by activated JAKs and required for dimerization (Imada et al., 2000).

After IFNγ binds to its receptors, receptor associated JAKs come into close proximity (Qian et al,. 2018). This allows for the JAKs to phosphorylate each other on their tyrosine residues (Figure 2). This process increases the activity of their kinase domains. These activated JAKs then phosphorylate tyrosine residues on the receptor allowing for the binding of proteins containing the SH2 domains (Imada et al., 2000). As mentioned before, STATs contain their SH2 domain that allow them to bind to the receptor. The STATs are then phosphorylated on its tyrosine residue by the activated JAKs (Imada et al., 2000). These phosphorylated STATs dimerize, translocate into the nucleus, and this allows them to exert their effects of gene regulation on IFN-stimulated Genes (ISGs) (Qian et al,. 2018).

One of the target genes is a gene that encodes Interferon Regulatory Factor 1 (IRF-1). This then leads to an upregulation of IRF-1 expression within the cell.

Figure 2: PD-L1 Activation Via JAK/STAT/IRF-1 Axis. The JAK-STAT pathway activation in a tumor cell during cross-talk with $CD8^+$ T-cells. The Cytotoxic T-Cell recognizes the tumor cell, secretes IFNγ, which then interacts with its receptor to activate JAK. JAK then phosphorylates STAT1. STAT1 dimerizes, moves to the nucleus, and upregulates transcription of genes such as the one that codes for IRF-1. IRF-1 upregulates the transcription of Programmed death ligand 1 (PD-L1). PD-L1 is expressed on the surface of the tumor cell to inhibit the function of the $CD8^+$ T-Cell, allowing for the tumor to evade the immune response.

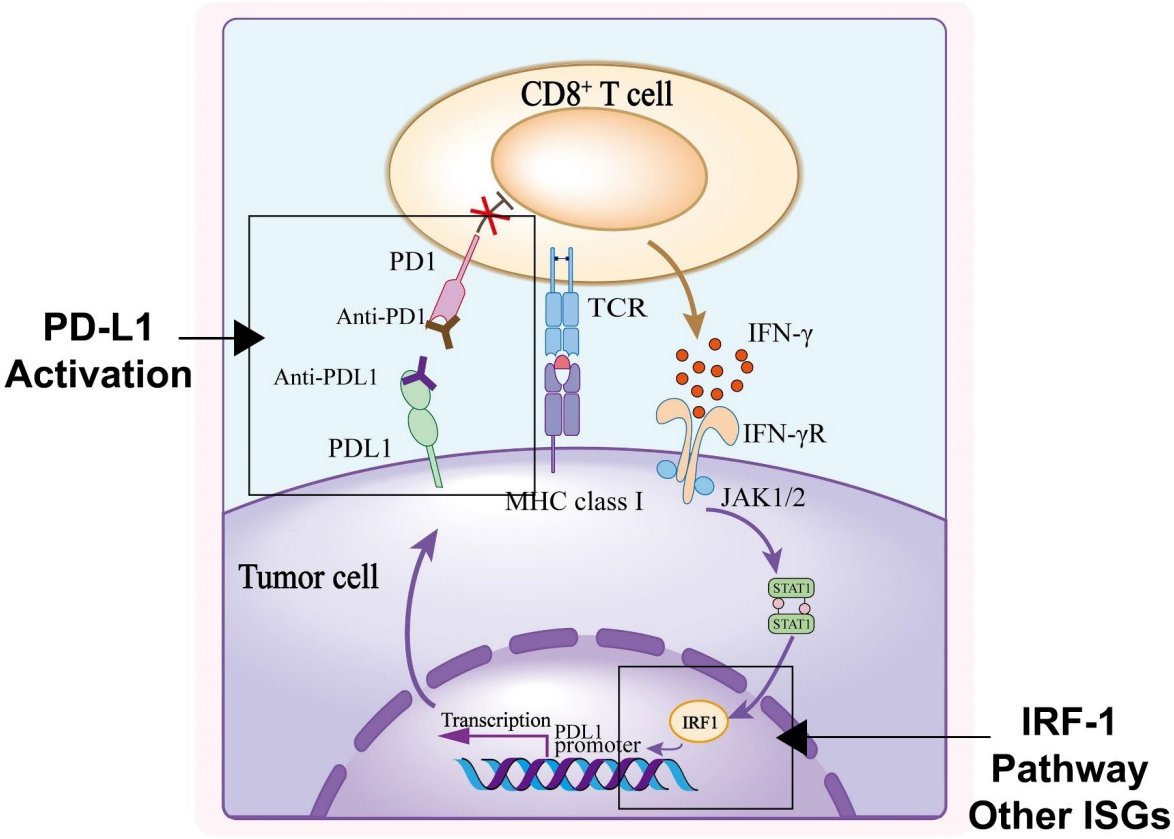

ADOPTED FROM: Lei Qingyang, Wang Dan, Sun Kai, Wang Liping, Zhang Yi, Resistance Mechanisms of Anti-PD1/PDL1 Therapy in Solid Tumors https://www.frontiersin.org/article/10.3389/fcell.2020.00672

Interferon Regulatory Factor 1 (IRF-1) has been shown to play a key role in IFNγ responses throughout the innate immune system (Liu et al,. 2005). Interferon Regulatory Factors (IRFs) modulate a series of downstream responses to pathogens. These IRFs regulate transcription of interferons and other innate immune system responses. IRF-1, IRF2, IRF4, and IRF8 play vital roles in development of immune cells including dendritic, myeloid, natural killer (NK) along with B and T Cells (Feng et al,. 2021).

IRF-1 is expressed at low basal levels in most human cells and its expression can be induced by different regulatory pathways. Low IRF-1 expression is linked to both unstable mRNA as the IRF-1 protein (Feng et al,. 2021). However, the stability of both the mRNA and the IRF-1 protein is dramatically increased in response to stimuli such as IFNγ. IRF-1 drives a powerful positive feedback loop, as it upregulates expression of ISGs (Karki et al,. 2021).

In a recent paper, it was shown that IRF-1 was vital for the recruitment of T-Cells to the brain during inflammation. IRF-1 drives the production of important chemokines, such as CXCL10 and CCL5, during immune responses (Harikumar et al,. 2014). Also within the brain, IRF-1 is vital for IFNγ mediated Major Histocompatibility Complex (MHC)-Class 1 gene expression in astrocytes (Jarosinski et al,. 2002).

The role of IRF-1 in cancer is more complicated. IRF-1 has been shown to modulate cellular responses that are involved in tumorigenesis (Karki et al,. 2020). NF-κB plays a key role in regulating the immune system responses to pathogens. Improper regulation of NF-κB can lead to chronic inflammation promoting cancer. Interestingly, TNF, known to activate NF-κB, also upregulates the expression of IRF-1. Engagement

TNF-α receptors (TNFR) has been shown to induce IRF-1. This drives an IRF-1-dependent positive feedback loop, leading to greater expression of IFNγ (Feng et al,. 2021).

This synergism of TNF-α and IFNγ can lead to inflammatory cell death. TNF-α and IFNγ activate the JAK/STAT1/IRF-1 axis, which in turn leads to an increase in nitric oxide production and increases Caspase 3 activity and PANoptosis (Pyroptosis, Apoptosis, and Necroptosis) (Karki et al,. 2020). Unfortunately, an upregulation of this axis is associated with a cytokine storm that induces PANoptosis medicated cell death and eventually leads to tissue damage (Karki et al,. 2020).

PANoptosis is a defense mechanism that is activated in infected cells. However, PANoptosis can also prevent tumorigenesis. PANoptosis has been shown to restrict tumorigenesis in spontaneous model of colorectal cancer under the control of IRF-1 (Karki et al,. 2020). On the other hand, IRF-1 also drives expression of programmed death-ligand 1 (PD-L1) in tumor cells, which has been shown to suppress the immune system responses (Figure 2) (Yi et al,. 2021).

However, the role of IRF-1 in PD-L1 expression in GBM has yet to be investigated.

Programmed death ligand 1 (PD-L1) is a transmembrane protein made up of an Ig variable distal region and an Ig constant proximal region (Escors et al,. 2018). PD-L1 interacts with PD-1+ receptors on T cells. The PD-1/PD-L1 interaction and signaling allows for cells to evade the immune system responses (Ostrand-Rosenberg et al,. 2014), with inhibition of cytokine release by T-cells and sometimes inhibition of their apoptosis. PD-L1 also downregulates NF-κB activation, which is important for immune responses and also cancer development (Scheffel et al,. 2021).

Expression of PD-L1 has been shown to be a major mechanism by which tumor cells avoid the immune system. This has been documented in various cancers and PD-L1 is already a target of various immunotherapies. In gastric carcinoma, the JAK2/STAT1/IRF-1 pathway drives overexpression of PD-L1 (Moon et al,. 2017). PD-L1 is also constitutively expressed on most carcinoma cells along with an overexpression in other cells, such as tumor associated dendritic cells that promote tumor growth and vascularization. Along with inhibiting T-cells response, PD-L1 downregulates responses of other immune cells, such as Natural Killer T Cells (NKTs) and B Cells (Ostrand-Rosenberg et al,. 2014).

In a recent study on traumatic brain injury, it was shown that PD-L1 expression may play a vital role suppressing immune system responses and subsequent tissue damage. PD-L1+ astrocytes exhibited immunosuppressive functions limiting post traumatic brain damage after secondary brain injury (Gao et al,. 2022).

Hence, the JAK/STAT/IRF-1 pathway in GBM-associated astrocytes may lead to the expression of PD-L1 and support the generation of immunosuppressive microenvironment.

MATERIALS AND METHODS

Mouse Development:

IRF-1$^{loxP/loxP}$ were bred with GFAP-CRE mice to generate IRF-1 astrocyte specific conditional knockout IRF-1$^{loxP/loxP, GFAP-CRE}$ (here referred as IRF-1 cKO mice). These mice were bred at Virginia Commonwealth University in accordance with Institutional Animal Care and Use Committee (IACUC) guidelines. These animals were housed in a room that provided a natural light and dark cycle, along with being provided standard laboratory chow and water. The animals chosen for the experiment were ones that were 8-12 weeks old and GFAP-CRE+, expressing CRE recombinase in astrocytes.

Plasmid Purification:

Bacteria containing the plasmids pLenti (H-RasV12-shp53) were spread upon LB bacterial plates. Single colonies were used to inoculate subsequent liquid cultures. The plasmids were isolated using a QIAGEN midi kit according to the manufacturer's protocol. After the plasmid isolation, the purity of the plasmids was measured. This was done on the Biorad Nano-Drop machine using absorbance peaks of 260nm and 280nm.

Lentiviral Titration:

An astrocyte-specific oncogenic lentivirus was used to upregulate tumorigenesis within the mice chosen for experimentation. This lentivirus, in correspondence with recombinase within GFAP+ cells, would allow for the upregulation of Ras and the downregulation of p53 (Figure 3). This would cause genomic instability, eventually leading to tumor development within the animal. The lentiviruses were packaged by co-transfection of HEK293TN cells with a lentiviral vector (H-RasV12-shp53) packaging plasmid (Addgene; psPAX2), and envelope plasmid (ADDgene; pMD2.G) using lipofectamine 2000. At approximately 24-72 hours after transfection, the virus containing supernatant was concentrated using the Lenti-X concentrator (Clontech), following the manufacture's protocol. At this point, the lentiviral stocks were re-suspended in serum free Dulbecco's Modified Eagle's Medium (DMEM) and flash frozen in liquid nitrogen and stored at -80^{o}C. In doing so, we were able to create a virus with titer level of 10^{7}, which was quantified by imaging the virus infected cells that gave off red florescence. Using a stereotaxic apparatus, we were able to properly inject the virus within the cortex of our mice under anesthesia. A 0.9 mm buff hole was drilled 0.5 mm posterior to Bregma, 2.33 mm to the midline and approximately 3 mm into the brain at the rate of 0.5 µl per minute. The mice were then monitored everyday post-op for symptoms of tumor development. These mice were observed and weighed over the course of 12-13 weeks.

Figure 3: Ras Inducing Oncogenic Lenti Virus. The model for oncogenic lenti viral modulation in the expression of Ras and p53. This is controlled by Cre-Recombinase in GFAP+ mice. This same model is used for the expression of GFP (Green Fluorescent Protein) to make the tumors visible under immunohistochemistry microcopy.

Perfusion and Brain Extraction:

The mice to be perfused were sedated in isoflourine and then flushed with a 0.9% NaCl solution for 6 minutes via cardia puncture. These brains were collected for qPCR analysis. Additional brains required for immunofluorescence had the added step of being perfused with 4% paraformaldehyde (PFA) for another 6 minutes to preserve the tissue. The brains were then sectioned for immunofluorescence.

Immunofluorescence:

The brains were placed in a small amount 4% PFA for preservation for 24 hours. After that they were transferred to a 30% sucrose and PBS solution for 48 hours. These were extracted from the solution and the cerebellum were cut off and removed as the primary focus of this research was on the cortex. They were then finally placed into an OCT block and frozen. The OCT blocks were then taken to the cryostat for sectioning into 10 μm sections that were collected on slides. These then underwent an immunostaining procedure. On the first day the slides were trimmed of excess OCT. They were then dipped into frozen-cold acetone for 10 minutes, and then dipped in a 1x PBS/Triton mix three times. This was followed by a blocking of the tissue in a PBS and 40% fish skin gelatin solution. These slides were then incubated with primary antibodies. We used antibodies to bind to a specific set of proteins ranging from IRF-1 (Santa Cruz Biotechnology), Ionized Calcium Binding Adaptor Molecule (IBA-1) (Cell Signaling), PD-L1 (Cell Signaling), Glial Fibrillary Acidic Protein (GFAP) (Cell Signaling), Cluster of Differentiation 31 (CD31) (Cell Signaling), and Aquaporin 4 (AQP4) (Cell Signaling). Once they sat in the

primary antibody for 24 hours, they were then washed in PBS solution for another 3 times. Finally, they were incubated again in basic blocking solution followed by 90 minutes in secondary antibodies conjugated to fluorophores. As the tumors already had the fluorescence of green, we were unable to use the wavelength of 488 nm and had to rely on the 594 nm and the 647 nm wavelengths. Once this final process was taken care of, they were finally mounted using a top film with a layer of vectashield containing DAPI and sealed with nail polish. The slides requiring four separate wavelengths were imaged using a confocal laser microscope (Zeiss LSM (710/800)) and the slides needing three wavelengths were imaged on a Keyance or Zeiss LSM (710/800) microscopes. Quantifying these final images in ImageJ was key in interpreting our results and developing our conclusion.

Hematoxylin and Eosin (H&E) Staining:

The slide sections were deparaffinized using two changes of xylene for 10 minutes each. This was followed by re-hydration of the tissue in two changes of 100% alcohol, 5 minutes each, one change 95% alcohol for 1 minute, and one change of 70% alcohol for 1 minute. These slides were then run under slow gentle tap water for 2 minutes. At this point, all slides were blocked using Mayer's Hematoxylin Solution (Nova Ultra) for 2 minutes which was followed up by another rinse under gentle tap water for 2 minutes. These were then again changed into 95% alcohol solution for 1 minute. Finally, they were stained with the Eosin Solution (Nova Ultra) for 45 seconds at which point they were rinsed again with 95% alcohol for 1 minute and two changes of 100% alcohol for 5 minutes each. This was

all cleared using two changes of xylene at five minutes each. A xylene based mounting medium was also used to mount the coverslips and get the slides ready for visualization.

RNA Isolation:

The brains were split into two hemispheres, tumor and non-tumor, flash frozen in liquid nitrogen, and promptly placed in a -80ºC freezer for preservation. The samples were then crushed in mortar and pestle placed on dry ice into a fine powder. Small samples of this powder were then resuspended in 1 ml of Trizol (Invitrogen). The samples were treated with 200 µl of chloroform, inverted, and centrifuged at 13,200 RPM for 15 minutes at room temperature. At this point, there was a phase separation that was observed. The 500 µl of the clear upper phase was removed and transferred to tubes containing 100 µl of chloroform. There tubes were vigorously shaken and centrifuged as described above. Another phase separation was observed, at which time 400 µl of this upper phase was transferred to new tubes, and 1 µl of molecular grade glycogen (Invitrogen) was mixed into solution. 500 µl of isopropanol was added, and the tubes were inverted multiple times and placed on ice. These tubes were centrifuged yet again at 13,200 RPM but this time for 10 minutes at 4°C. The supernatant that was collected was poured off to reveal a small white pellet at the bottom of each tube. At this point, 1 ml of cold 70% ethanol was added to each tube and centrifuged at 13,200 RPM for 10 minutes at 4°C. More supernatant was poured off and the ethanol wash and centrifugation steps were repeated one more time. Any remaining ethanol was pipetted out of the tube. The tubes were placed at 37 ºC to allow for

any excess ethanol to evaporate from the tube. The RNA were resuspended in 22 µl of DEPC H_2O.

RT qPCR:

After RNA isolation was completed, 1 µg of the RNA was reverse transcribed using a High-Capacity cDNA Archive kit (Applied Biosystems). 1:10 and 1:100 dilutions of the cDNA were created to be used in qPCR analysis. Master mix was created for each target primer that was to be tested for using 4 µl of DEPC H_2O, 10 µl PowerUp SYBR Green Master Mix (Applied Biosystems), and 1 µl of the primer sets per sample. Since the samples were run in duplicates on the qPCR plate, double of the master mix was created per primer. 15 µl of master mix was added to each well. 5 µl of each sample was added to the wells containing the master mix from before at which point the plates were sealed and centrifuged for 1 minute. The mixtures were analyzed using a CFX Connect Real Time System Thermal Cycler (Bio-Rad). The samples were held at 95°C for 30 seconds to start. The samples were then cycled from 95°C for 10 seconds down to 60°C for 30 seconds. The plate was read, and the cycle was repeated 39 more times. The 1:100 dilution of cDNA was used to evaluate GAPDH expression which was used as a control in subsequent quantification. The expression of genes of interest were measured using the 1:10 dilution of cDNA. For the quantification, the WT non-tumor hemisphere was held as a control for the other hemisphere groups.

Quantification and Analysis:

To quantify the different results, different methodologies were applied for immunofluorescence and qPCR. For each antibody, a positive signal was assigned a unique number of pixels using ImageJ (Fiji). For example, PD-L1 was at 12 pixels for one puncta expression, whereas IBA-1 was at 120 pixels. At this point, a box was drawn in the location of interest, may that be within the tumor, on the edge, slightly around the tumor. Puncta Analyzer was run in ImageJ (Fiji) with the definition of a puncta expression being set the level of pixels we quantified previously. This tool measured all puncta that were above this threshold. To account for any background interference, the brightest image was used to set a level of threshold for intensity. This manner of quantification was kept the same across the cKO and WT brains for each specific staining. For qPCR, the data was first normalized using GAPDH and then analyzed using the delta-delta Ct method. This information was then uploaded to GraphPad Prism for further statistical testing. Statistical analysis of both qPCR and this puncta data was done within GraphPad Prisim. T-Tests were run to evaluate the different levels between hemispheres of interest and then plotted for visualization with error bars.

RESULTS

Deletion of IRF-1 from astrocytes had no significant effect on tumor generation nor growth.

IRF-1 has been shown to be induced by the JAK-STAT pathway. The JAK-STAT pathway is activated in GBM associated astrocytes, which are a critical component of the microenvironment. IRF-1 has also been shown to upregulate PD-L1 in other cancers. To test if astrocytic IRF-1 is important in glioma growth and immune system suppression, we used IRF-1$^{LoxP/LoxP;\ GFAP\text{-}CRE+}$ mice which allowed us to specifically knockout IRF-1 from astrocytes using CRE Recombinase. We used a oncogenic lentivirus that underwent recombination in GFAP+ cells. This allowed for us to create our spontaneous glioma model. In doing so, deletion of the FLOXed alleles and simultaneous recombination of the virus that only occurs in GFAP+ cells (astrocytes) allowed for the expression of Ras and the downregulation of p53. These events promoted proliferation and genomic instability, eventually leading to tumorigenesis. The recombination also allowed for the expression of GFP within gliomas enabling visualization. We hypothesized the loss of IRF-1 would lead to an increase in the anti-tumor immune responses via cytotoxic T-Cells. This would shunt tumor growth in the IRF-1 cKO mice. The mice were assumed to have tumors when they started losing weight while also neglecting general grooming practices. At this point they were perfused, and we confirmed whether they had a tumor or not. Surprisingly, the deletion of IRF-1 had no significant difference on tumor generation nor growth (Figure 4,5). The mice all had similar tumor incident rates (Figure 4) as well survival rate upon

diagnosis (Figure 5). This surprising result suggest that the loss of IRF-1 does not have an effect on the actual tumor generation nor survival.

Figure 4: Tumor Incident Rate. Tumor incidents in WT and IRF-1 cKO mice within 12 weeks of lentiviral injection. n=9,11; p=0.1824, T-Test

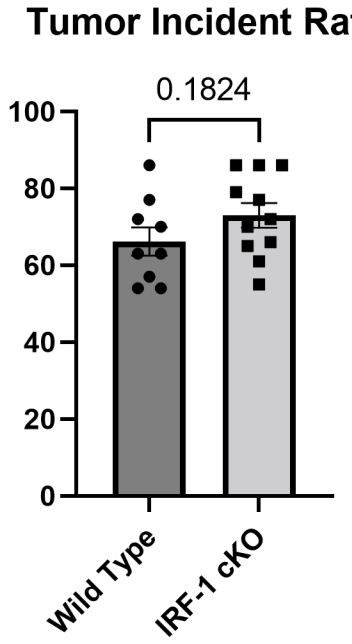

Figure 5: Tumor Survival Rate. Survival rates of WT and IRF-1 cKO mice. p=0.3163, multiple T-Test

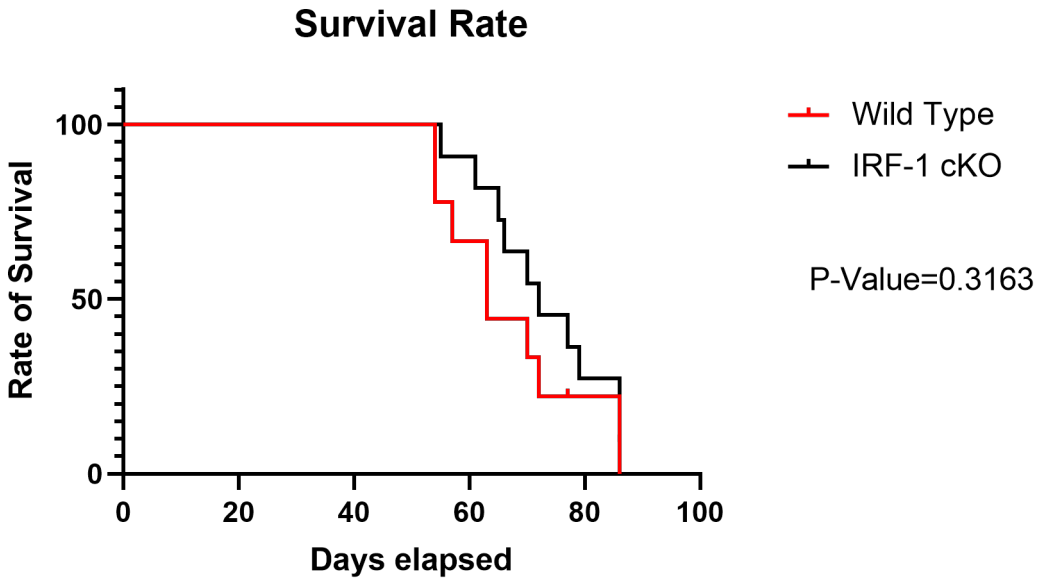

Spontaneous WT and cKO gliomas had similar histology.

We analyzed gliomas generated in WT and IRF-1 cKO animals. First, these spontaneous gliomas generated in WT and IRF-1 cKO mice were similar when stained with H&E (Figure 6A). These tumors were highly invasive, with groups of glioma cells invading surrounding healthy brain tissue. Second, we could easily visualize glioma cells due to the expression of GFP in both subsets of mice brains, suggesting that recombination of lentivirus occurred in both WT and IRF-1 cKO mice (Figure 6B).

Figure 6: Morphology of Tumor Growth. Similar morphology and GFP expression of gliomas in WT and cKO mice. Captured at 2x for full brain and 20x for close up. **(A)** H&E **(B)** Green, GFP; Blue, DAPI

A

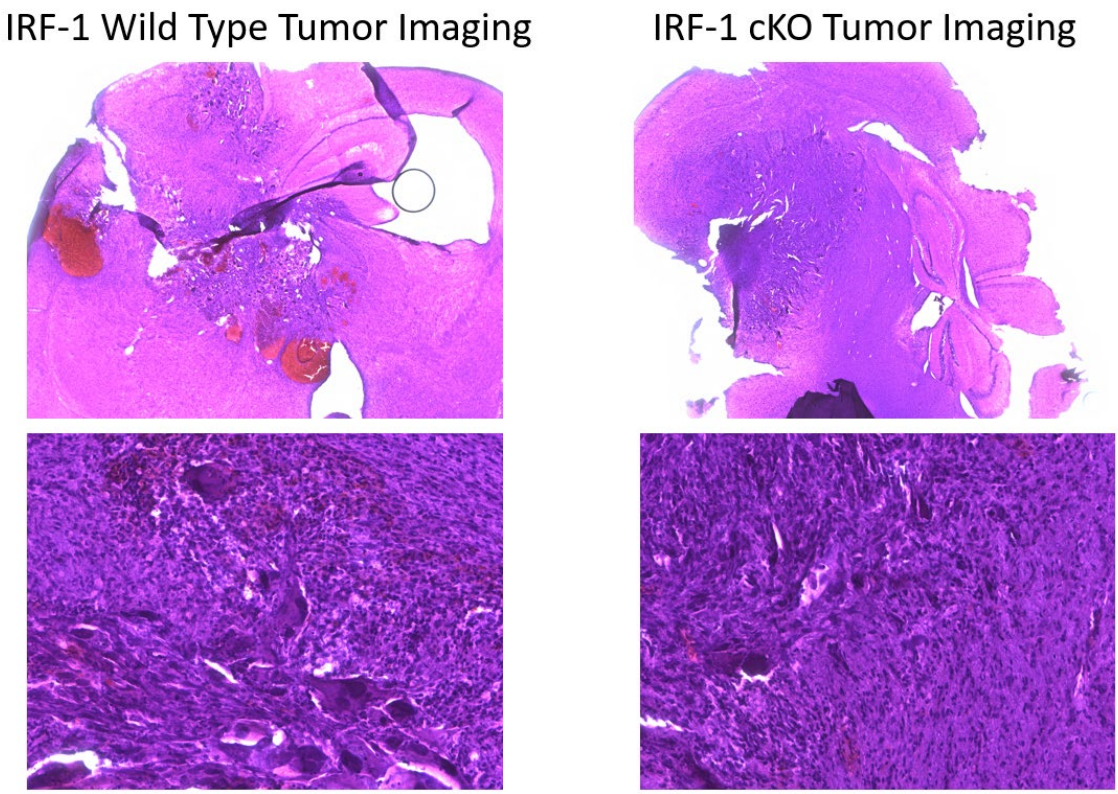

B

IRF-1 Wild Type Tumor Imaging

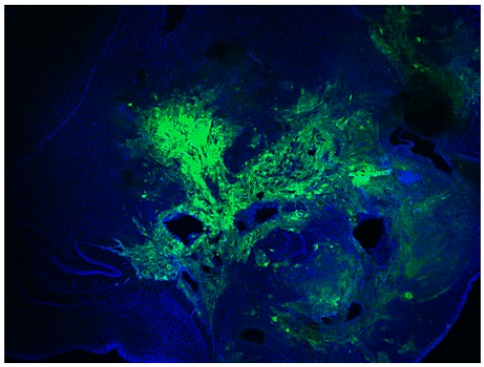

IRF-1 cKO Tumor Imaging

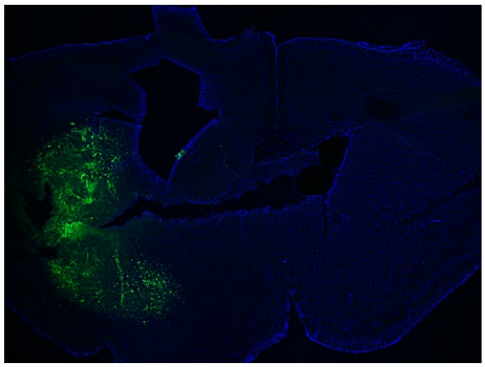

Significant decrease in IRF-1 expression within the tumors of IRF-1 cKO brains.

To confirm that IRF-1 had been knocked out, the slides were immunostained for IRF-1. As expected, there was significantly lower levels of IRF-1 (RED) staining within the tumor but not as around the tumors in IRF-1 cKO mice (Figure 7A). These have been quantified using ImageJ. ImageJ (Fiji) boxes of equal size were created within and right next to the tumor. These boxes were analyzed for the number of positive puncta. We first took a puncta assumed to represent a positive staining and found the number of pixels within. This size of pixelated puncta was set as standardized puncta. Subsequently, we analyzed the area within and around the tumor for the number of standardized puncta. There was a significant decrease of IRF-1 puncta within the tumor or IRF-1 cKO mice (Figure 7B). However, this was not the case when it came to the area around the tumor, and there was no significant difference in IRF-1 expression between tissue surrounding tumors in WT and IRF-1 cKO mice (Figure 7C). As a control, the non-tumor bearing hemispheres were also immunostained for IRF-1 (RED) (Figure 8A). There was no significant difference in IRF-1 expression between non-tumor hemispheres of WT and IRF-1 cKO mice (Figure 8B).

Figure 7: Loss of IRF-1 Expression Within the Tumor of IRF-1 cKO Mice. A) Keyance images of brain sections (20x) IRF-1 (RED), Glioma cells (GFP, GREEN), Nuclei (DAPI, BLUE) **B)** Quantification of **(A)** within the tumor **(B)** and in the surrounding tissue **(C)**. n=6,6, p=0.0399, T-Test **(B)**, and p=0.8124, T-Test **(C)**

A

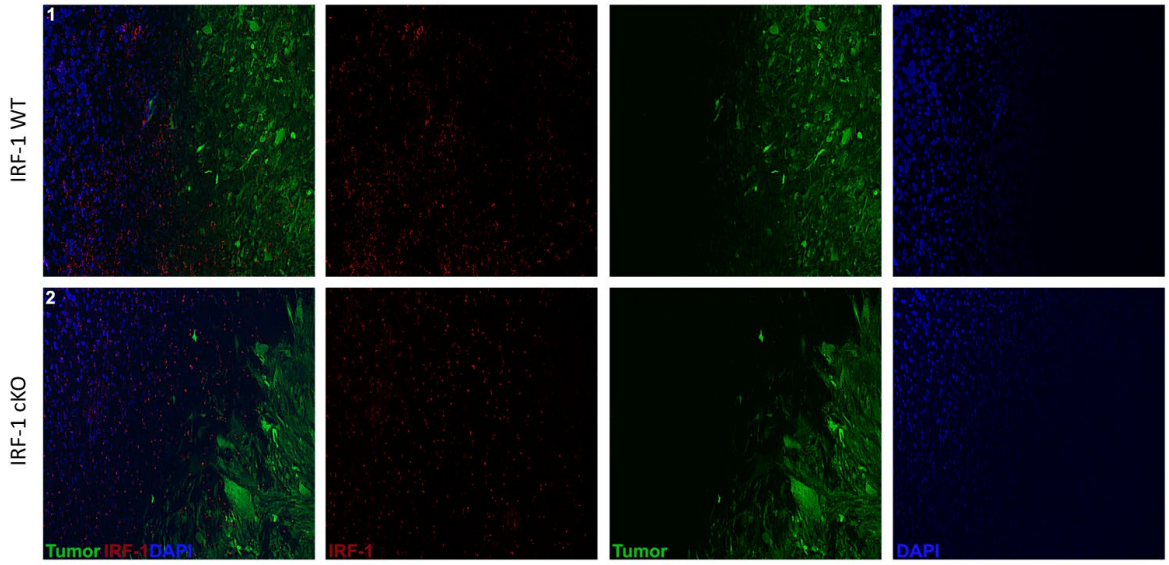

B

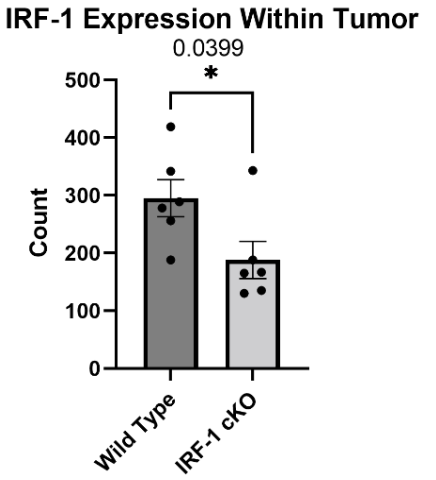

C

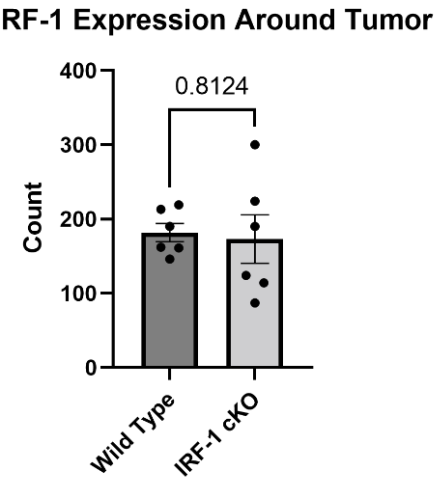

Figure 8: Equal Expression of IRF-1 in Non-Tumor Hemisphere of WT and IRF-1 cKO Mice. A) Keyance images of non-tumor hemisphere of WT and IRF-1 cKO mice within brain sections (20x) IRF-1 (RED), Glioma cells (GFP, GREEN), Nuclei (DAPI, BLUE). **B)** Quantification of **(A)**. n=4,4, p=0.1132, T-Test

A

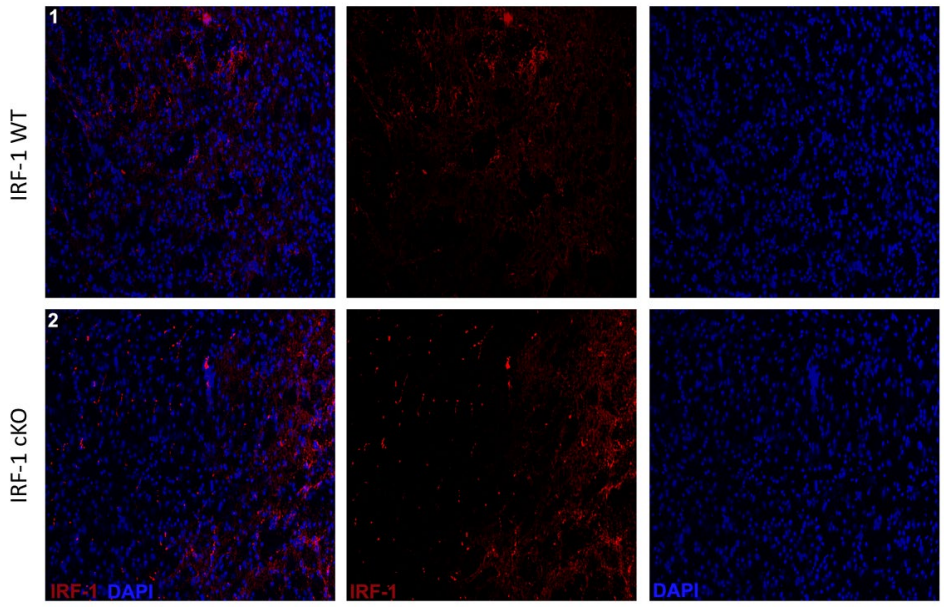

B

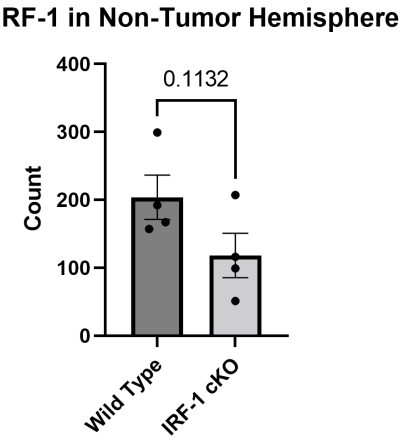

PD-L1 expression is downregulated in tumors of IRF-1 cKO mice.

It has been shown that IRF-1 regulates PD-L1 in several cancer cell types. Higher expression of IRF-1 can be upregulated via the JAK/STAT pathway. Therefore, we examined whether PD-L1 is affected by deletion of IRF-1 in astrocytes and glioma cells. We stained the sections for PD-L1 (RED) (Figure 9A). We found a significant difference between PD-L1 expression within the tumor but not in the surrounding tissue in IRF-1 cKO mice. The images were quantified by measuring the colocalization of red and green puncta within the tumor (Figure 9B) and only red around the tumor (Figure 9C). The lower expression of PD-L1 in the tumor can be explained by the lack of IRF-1 in glioma cells. However, the surrounding tissue contains many cells type of which only astrocytes had depleted IRF-1. The comparable expression of PD-L1 in the tissue around the tumor could be explained by IRF-1-dependent expression of PD-L1 by myeloid cells.

Figure 9: The Decreased Expression of PD-L1 in Gliomas of IRF-1 cKO Mice.

A) Confocal images of brain sections (20x) PD-L1 (RED), Glioma cells (GFP, GREEN), Nuclei (DAPI, BLUE) **B)** Quantification of **(A)** within the tumor **(B)** and in the surrounding tissue **(C)**. n=11,11, p=0.0446, T-Test **(B)**, and p=0.7855, T-Test **(C)**

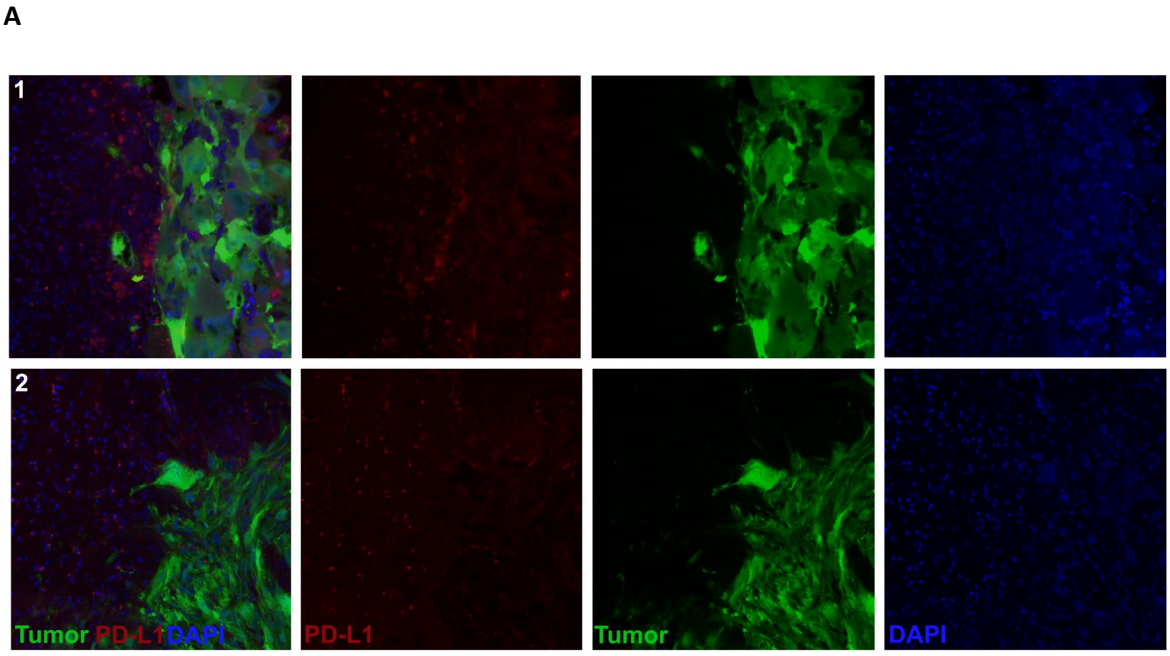

To further confirm and evaluate the downregulation of PD-L1 in the tumors of IRF-1 cKO mice, we analyzed its expression by qPCR. Expression in WT tumor hemispheres, WT non-tumor hemispheres, IRF-1 cKO tumor hemispheres, and IRF-1 cKO non-tumor hemispheres was examined (Figure 10). PD-L1 mRNA expression was significantly upregulated in the wild type hemispheres containing the tumor (Figure 10). In contrast, PD-L1 mRNA expression was only partially increased in the tumor containing hemisphere of the IRF-1 cKO mice. Nevertheless, there was no significant difference between PD-L1 mRNA expression between the glioma containing hemispheres of WT and IRF-1 cKO mice. This could be the result of significant PD-L1 expression in the tissue around the tumor.

Figure 10: PD-L1 mRNA Expression in the Brains of WT and IRF-1 cKO Mice.

Expression was analyzed by qPCR in the glioma bearing and glioma free hemispheres of WT and cKO mice. Data was analyzed by Two-Way ANOVA. n=4,4,4,4. p=0.1341.

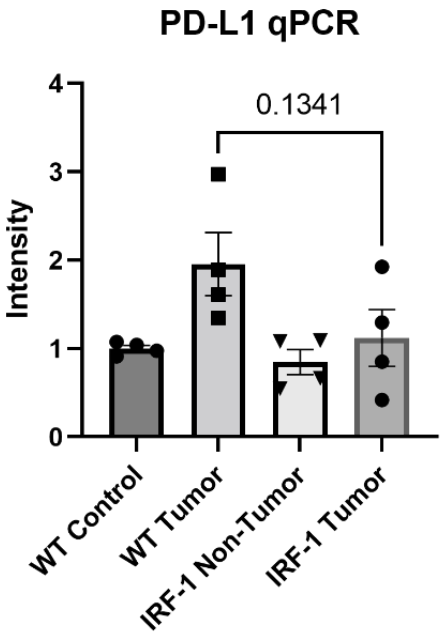

Significant downregulation of PD-L1 expression in astrocytes at the edge of the tumor.

As stated before, astrocytes play a critical role in the development of the immunosuppressive microenvironment in GBM. The crosstalk between astrocytes, microglia, and GBM cells allows for the establishment of this microenvironment. To examine the astrocyte-specific expression, the sections were co-stained for PD-L1 and GFAP (Figure 11A). PD-L1 and GFAP colocalization was examined at the edge of the tumor. We found that PD-L1 expression within the astrocytes was significantly decreased in the IRF-1 cKO mice (Figure 11B). This downregulation of PD-L1 expression was specific to the astrocytes at the tumor edge since there was no difference between the levels of PD-L1 expression within astrocytes further away from the tumor (Figure 11C). This suggests that the astrocytes at the edge of the tumor may upregulate PD-L1 via the IRF-1 axis. To confirm this finding, PD-L1 expression was examined in the astrocytes of the non-tumor hemispheres (Figure 12A). Puncta analysis indicated that there was no difference between the level of PD-L1 expression in astrocytes of the non-tumor bearing WT and IRF-1 cKO hemispheres (Figure 12B).

Figure 11: Expression of PD-L1 in Astrocytes Nearby the Tumor A) Confocal images of brain sections (20x) PD-L1 (RED), GFAP (YELLOW), Glioma cells (GFP, GREEN), Nuclei (DAPI, BLUE) **B)** Quantification of **(A)** within the tumor **(B)** and in the surrounding tissue **(C)**. n=6,6, p=0.02234, T-Test **(B)**, and p=0.1270, T-Test **(C)**

A

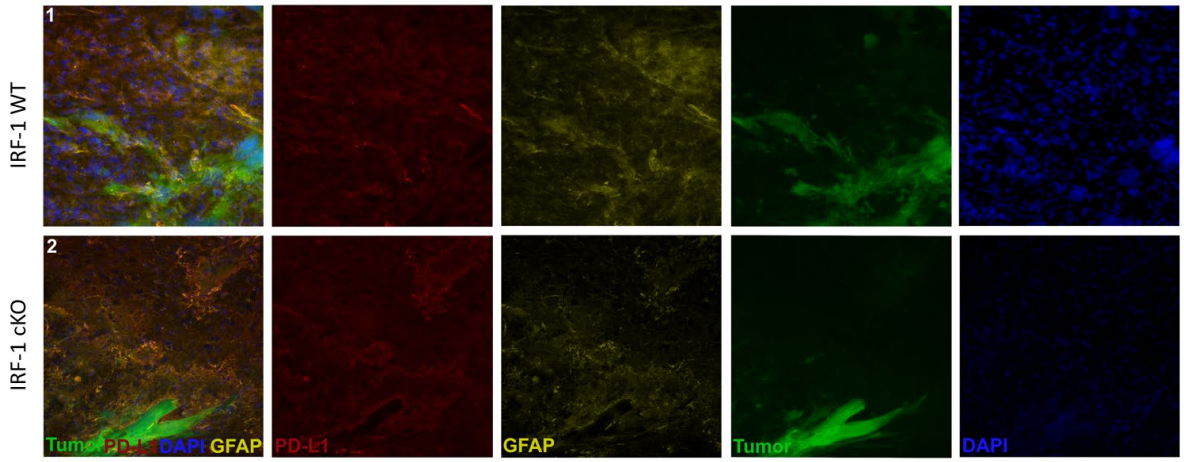

B

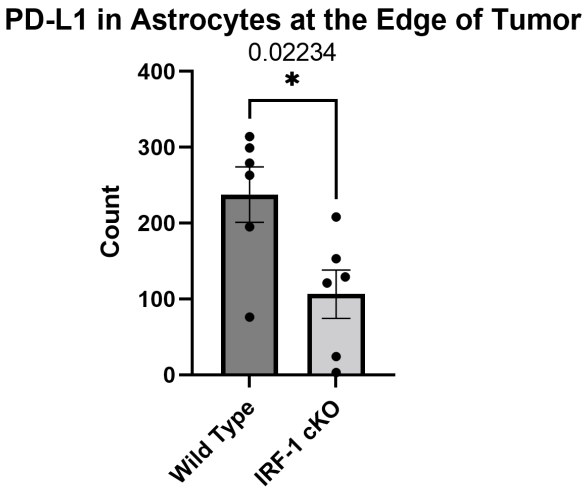

C

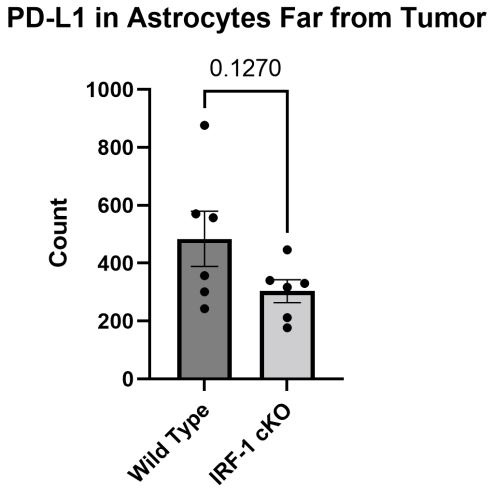

Figure 12: Expression of PD-L1 in Astrocytes of Non-Tumor Bearing Hemisphere. **A)** Confocal images of non-tumor hemisphere of WT and IRF-1 cKO mice within brain sections (20x) PD-L1 (RED), GFAP (YELLOW), Glioma cells (GFP, GREEN), Nuclei (DAPI, BLUE). **B)** Quantification of PD-L1 expression in the non-tumor bearing hemispheres. n=3,3, p=0.4647, T-Test **C)** Quantification of PD-L1 expression in astrocytes (GFAP) of the non-tumor bearing hemispheres. n=3,3, p=0.5696, T-Test

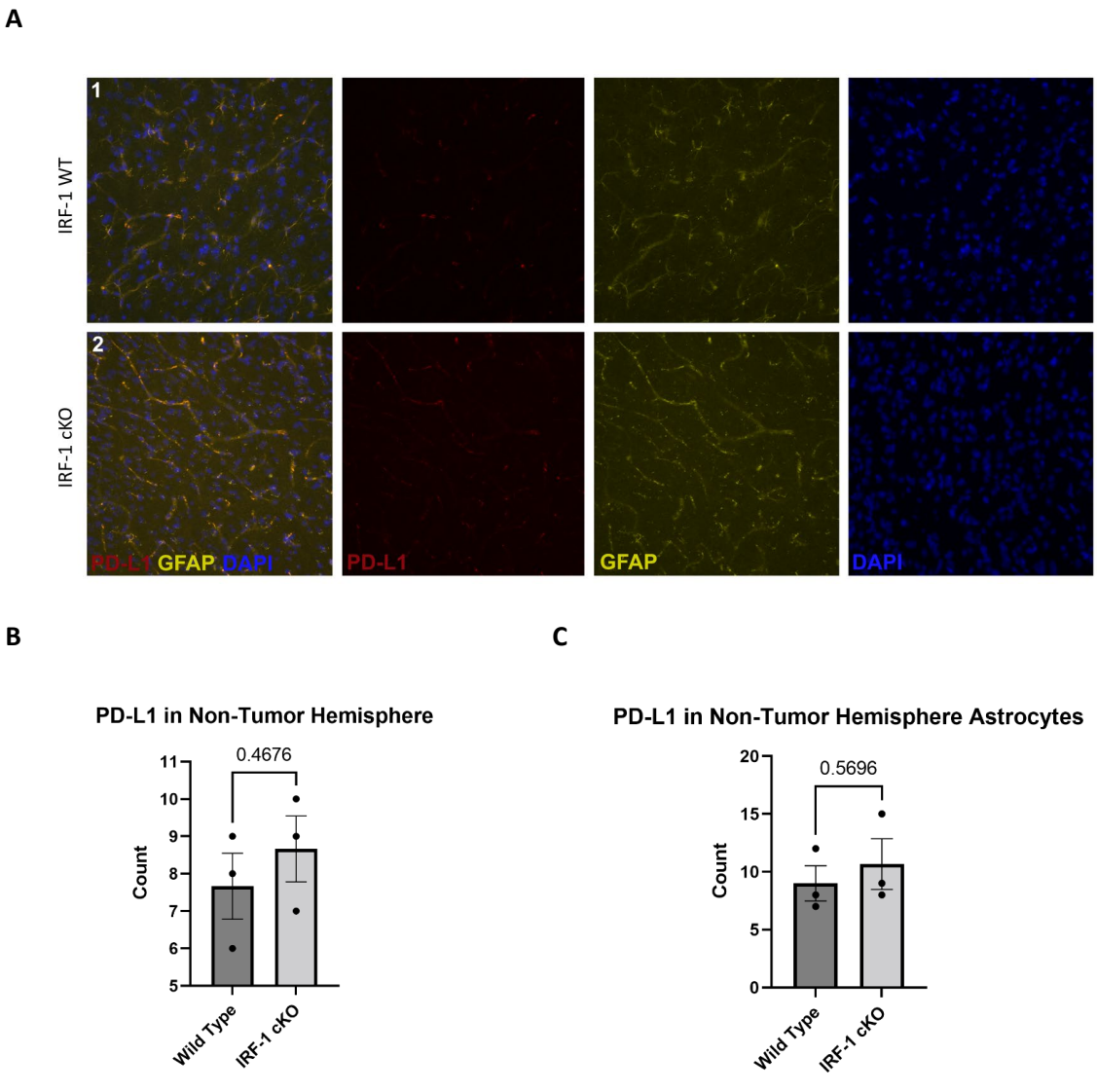

Similar expression of PD-L1 in tumor associated and proximal myeloid cells of WT and IRF-1 cKO mice.

PD-L1 expression was similar around the tumor in WT and IRF-1 cKO mice. However, PD-L1 expression was decreased in astrocytes on the edge of the tumor in IRF-1 cKO mice. This could be explained by high PD-L1 expression by other cell types, including myeloid cells, known to express PD-L1. We subsequently evaluated its expression in tumor associated microglia/macrophages. We examined PD-L1expression in IBA-1 positive cells (Figure 13A). We quantified co-localized puncta within the tumor and the area around the tumor. We found that there were similar levels of PD-L1 expression in myeloid cells with the tumor and the area surrounding the tumor (Figure 13B, C). Since IRF-1 was deleted only in astrocytes of IRF-1 cKO mice, comparable level of PD-L1 expression in myeloid cells seems to adequately explain lack of differences in the expression of PD-L1 in the area surrounding the tumor. Furthermore, we concluded that myeloid PD-L1 expression is independent of IRF-1 signaling in astrocytes and glioma cells.

Figure 13: PD-L1 Expression in Myeloid Cells Around the Tumor A) Confocal images of brain sections (20x) IBA-1 (RED), PD-L1 (YELLOW), Glioma cells (GFP, GREEN), Nuclei (DAPI, BLUE) **B)** Quantification of **(A)** within the tumor **(B)** and in the surrounding tissue **(C)**. n=6,6, p=0.6912, T-Test **(B)**, and p>0.9999, T-Test **(C)**

A

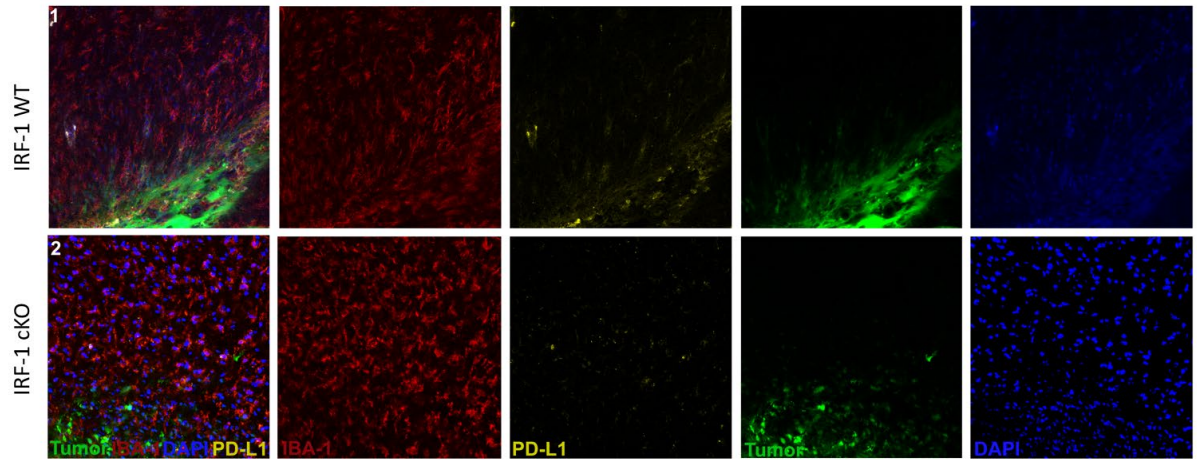

B

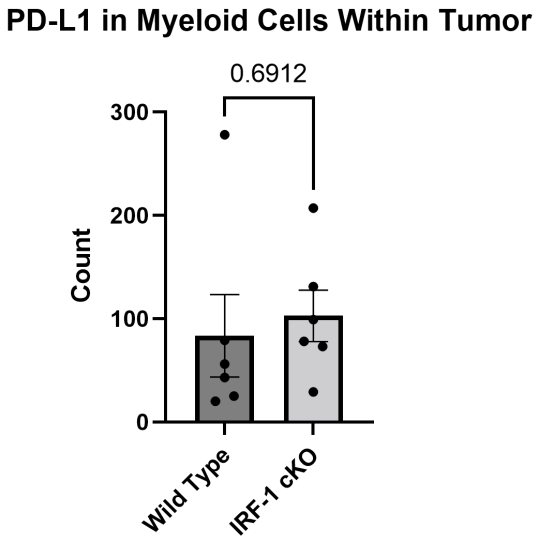

C

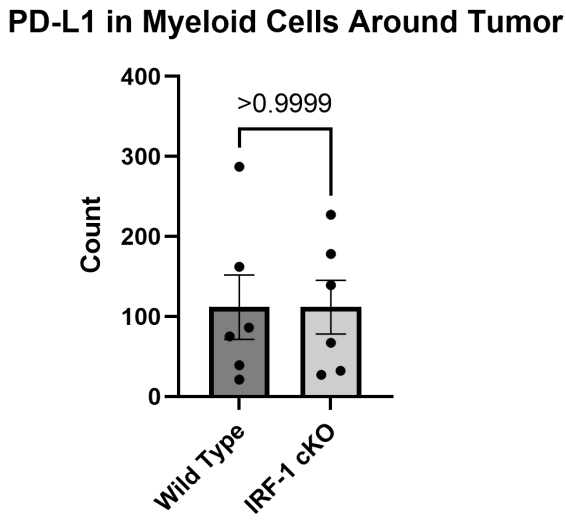

Similar number of IBA-1 positive cells within tumor and the area around it.

We next evaluated the number of myeloid cells in the tumor microenvironment using IBA-1 staining, which detects both microglia and monocyte-derived macrophages (Figure 14A). We expected no difference since PD-L1 is known to decrease the number of $CD8^+$ Cytotoxic Anti-Tumor T-Cell, but not myeloid cells abundance. Indeed, there was no significant difference in the number of IBA-1 positive cells within the tumors of WT and IRF-1 cKO mice (Figure 14B). This was also similar to the results that were observed around the tumors. There was also no significant difference in IBA-1 expression around the tumor of WT and IRF-1 cKO mice (Figure 14C). To further confirm this data we examined expression of known markers of myeloid cells, C1QA and CD68. Both of these proteins are highly expressed by circulating and in resident myeloid cells. There was no significant difference between the level of mRNA expression for these markers between the tumor hemispheres of the WT and IRF-1 cKO brains (Figure 15A, B). We also examined expression of Cx3CR1, which is specifically expressed by microglia, at high levels. Although Cx3CR1 expression was higher in hemispheres containing tumors there was no difference between WT and IRF-1 cKO mice (Figure 15C). Finally, we also examined other tumor markers such as Interleukin-10 (IL-10), which has also been implicated in downregulation of the immune responses, and Lipocalin-2 (LCN2), which is a key regulator of the immune system. Although IL-10 and LCN2 expression was higher in hemispheres containing tumors, there was no significant difference between WT and IRF-1 cKO (Figure 15D, E).

Figure 14: Myeloid Cells in the Tumor Vicinity A) Confocal images of brain sections (20x) IBA-1 (RED), Glioma cells (GFP, GREEN), Nuclei (DAPI, BLUE) **B)** Quantification of **(A)** within the tumor **(B)** and in the surrounding tissue **(C)**. n=6,6, p=0.8124, T-Test **(B)**, and p=0.2447, T-Test **(C)**

A

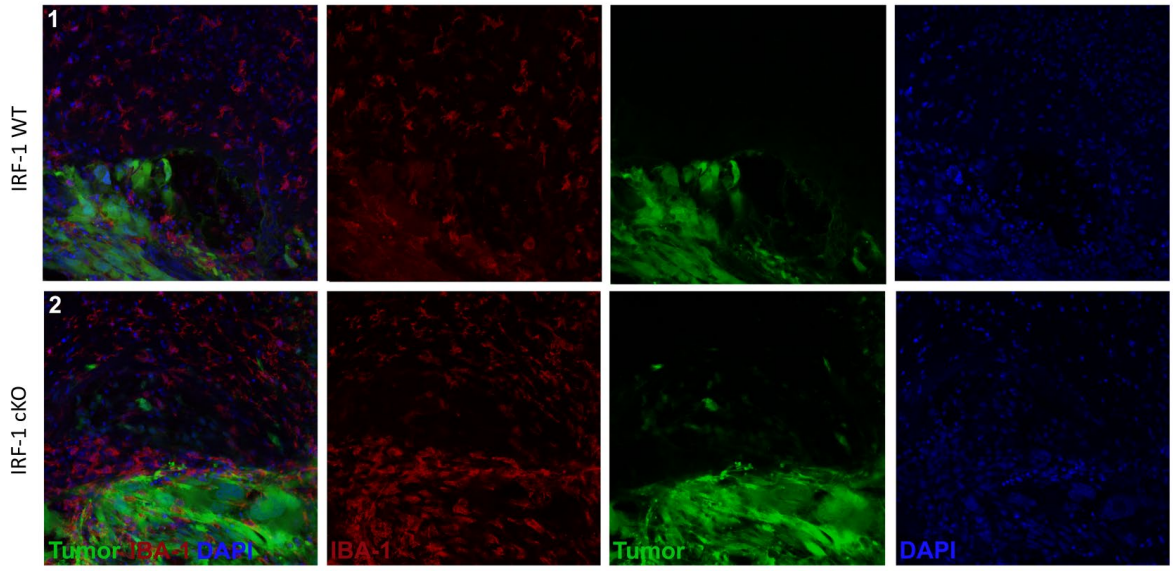

B

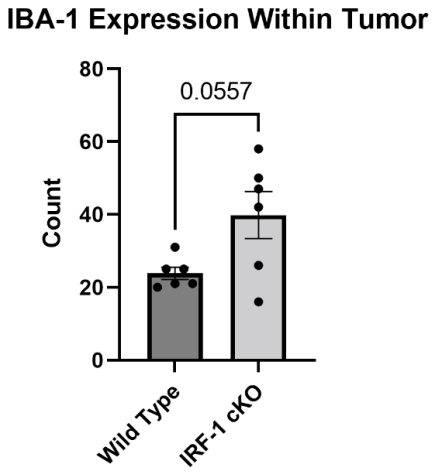

C

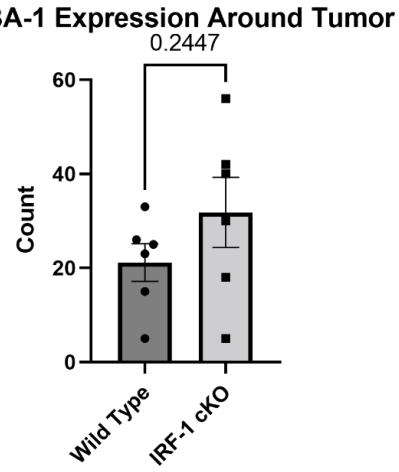

Figure 15: Expression of genes by myeloid cells in WT and IRF-1 cKO mice.

C1QA(A), CD68(B), Cx3CR1 (C), IL-10(D) and LCN2(E). Expression was analyzed by qPCR n=4,4,4,4, Two-Way ANOVA.

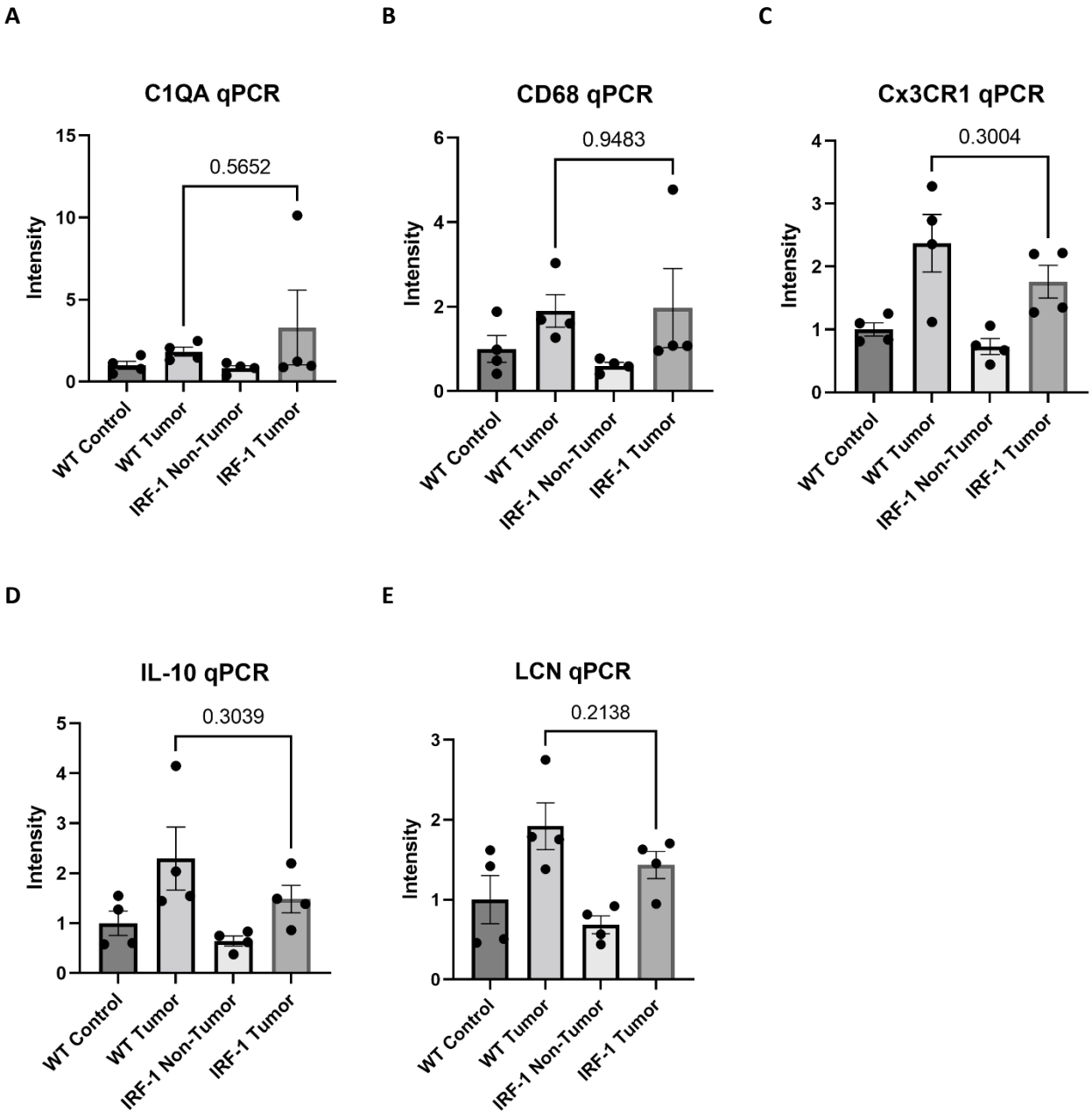

Astrocytic IRF-1 deficiency affects vascularization of gliomas.

Subsequently, we examined vascularization of gliomas since astrocytes control blood vessels via their end feet, and vascularization is critical for tumor growth. CD31 or Platelet Endothelial Cell Adhesion Molecule (PECAM-1) is a cell-to-cell adhesion protein expressed on endothelial cells. CD31 facilitates new blood vessel formation via the cell-to-cell adhesion function it provides. CD31 is abundantly expressed on endothelial cells but also at lower levels on, platelets, macrophages, Kupffer cells, granulocytes, lymphocytes, and osteoclasts. There was a significant difference between the levels of CD31 staining between WT and IRF-1 cKO tumor bearing hemispheres, with a significant downregulation within the cKO brains (Figure 16A, B, C). The vascularization of both the tumor and its environment was diminished in IRF-1 cKO tumor bearing hemispheres. We also examined the expression of Vascular endothelial growth factor (VEGF) known to regulate vascularization (Figure 17). WT tumors induced upregulation of VEGF expression within the hemispheres containing the tumor, which was not evident in IRF-1 cKO tumor bearing hemispheres. Nonetheless, there was no significant difference in VEGF expression between WT and IRF-1 cKO tumor bearing hemispheres. Finally, we analyzed expression of CD31 in the non-tumor hemispheres (Figure 18A). There was no significant difference in expression of CD-31 within the non-tumor hemisphere between the WT and IRF-1 cKO mice (Figure 18B). We concluded that deletion of IRF-1 from astrocytes affects tumor vascularization.

Figure 16: CD31 Expression in the Tumor Vicinity. A) Keyance images of brain sections (20x) CD31 (RED), Glioma cells (GFP, GREEN), Nuclei (DAPI, BLUE) **B)** Quantification of **(A)** within the tumor **(B)** and in the surrounding tissue **(C)**. n=7,10, p=0.004, T-Test **(B)**, and p<0.00001, T-Test **(C)**

A

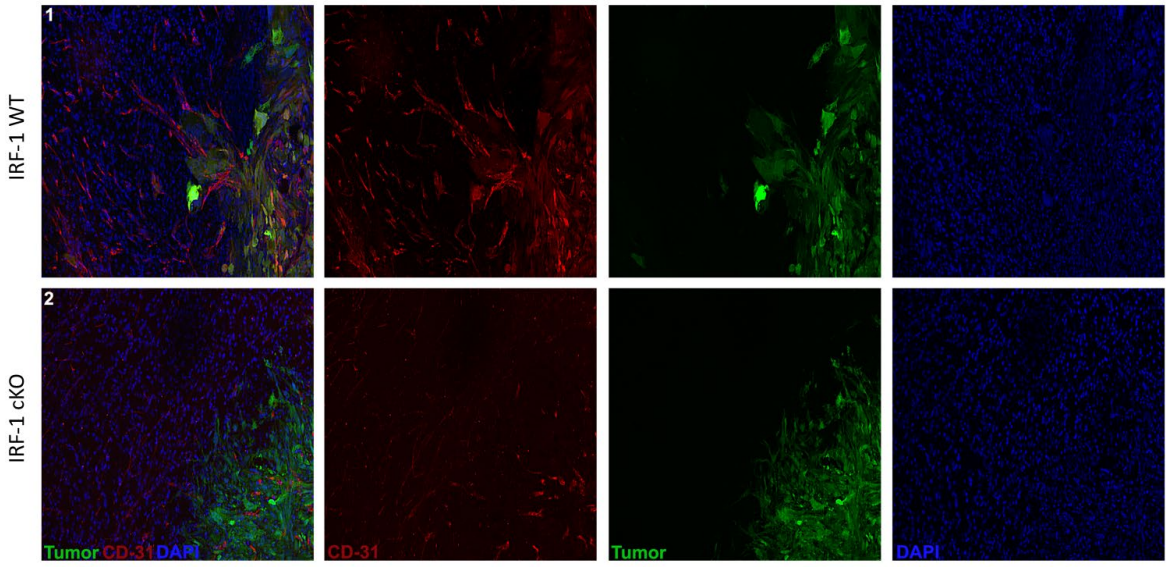

B

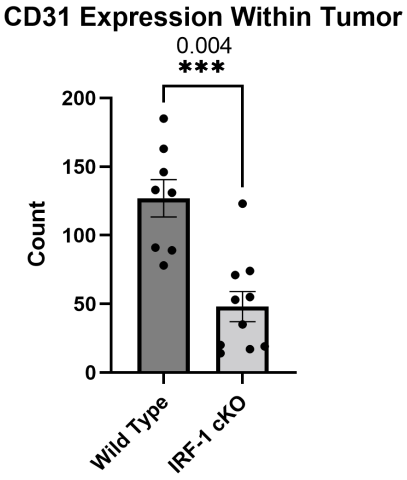

C

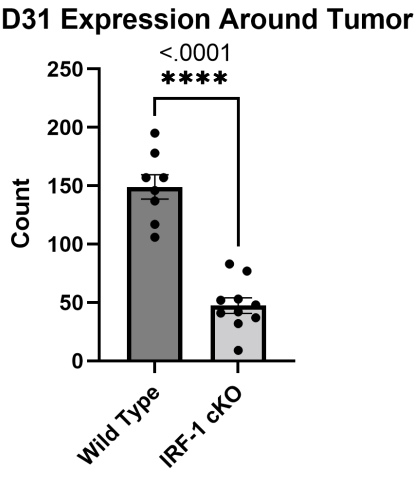

Figure 17: Expression of VEGF in WT and IRF-1 cKO mice. Expression was analyzed by qPCR. N=4,4,4,4, p=0.1050, Two-Way ANOVA

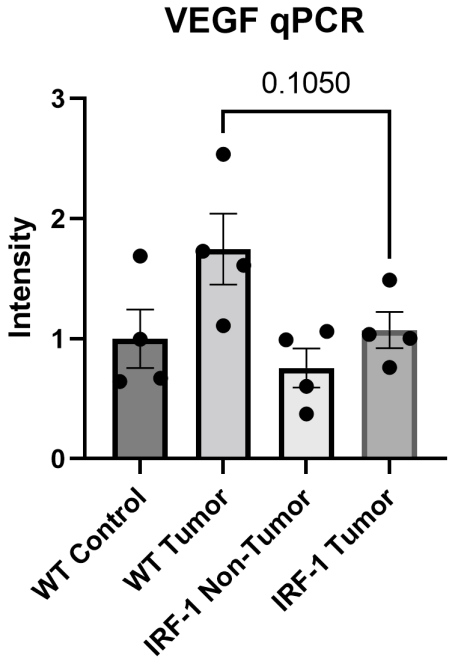

Figure 18: CD31 Staining in the Non-Tumor Bearing Hemisphere. A) Keyance images of non-tumor bearing hemisphere sections of WT and IRF-1 cKO (20x) CD31 (RED) and Nuclei (DAPI, BLUE) **B)** Quantification of **(A)** n=4,4, p=0.9107, T-Test

A

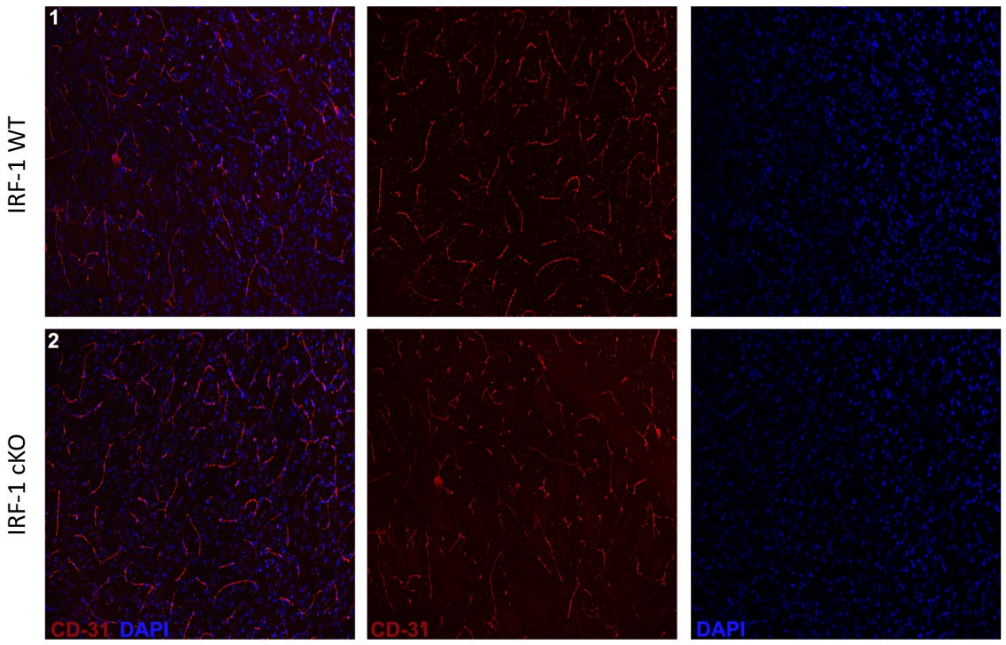

B

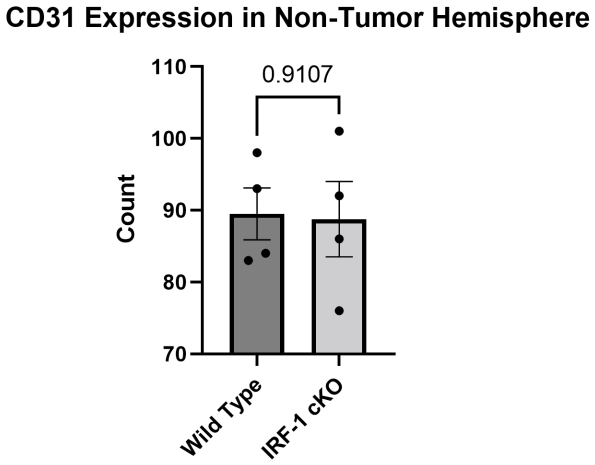

Aquaporin-4 expression is downregulated in IRF-1 cKO harboring gliomas.

Since astrocyte end feet are important in the control of vascular events, we examined expression of AQP4 known to be critical for end feet function. The AQP4 forms a channel that facilitates water movement in the vicinity of cerebrospinal fluid and vasculature. Since CD31 expression suggested defective vascularization of IRF-1 cKO mice, we suspected that AQP4 expression may also be affected. We analyzed AQP4 expression between the WT and IRF-1 cKO mice (Figure 19A). There was a significant downregulation in AQP4 expression within the IRF-1 cKO tumor bearing hemispheres (Figure 19B). There was a slight downregulation of AQP4 expression in the area around the tumor; however, this was not statistically significant (Figure 19C). Finally, we analyzed the expression of AQP4 within the non-tumor hemispheres (Figure 20A, B). There was no significant difference in AQP4 expression between WT and IRF-1 cKO non-tumor bearing hemispheres. We concluded that IRF-1 deletion within astrocytes and tumor cells diminishes vascularization within the tumor likely through affecting astrocytic endfeet function.

Figure 19: AQP4 Expression in the Tumor Vicinity. A) Confocal images of brain sections (20x) AQP4 (RED), Glioma cells (GFP, GREEN), Nuclei (DAPI, BLUE) **B)** Quantification of **(A)** within the tumor **(B)** and in the surrounding tissue **(C)**. n=6,6, p=0.0399, T-Test **(B)**, and p=0.7467, T-Test **(C)**

A

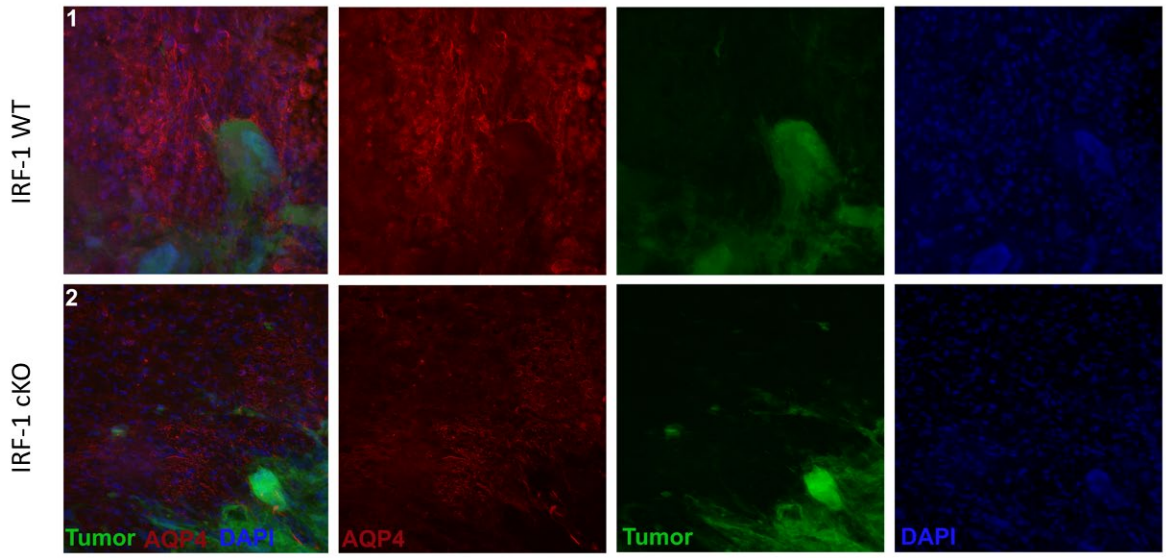

B

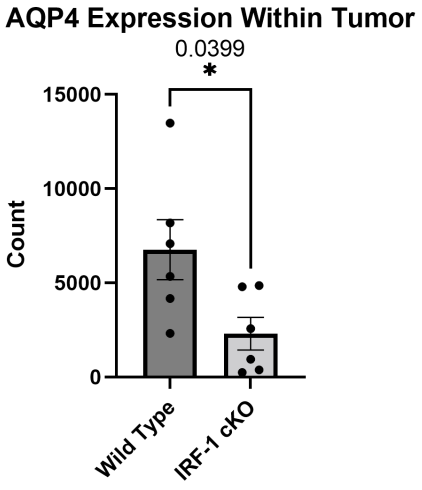

C

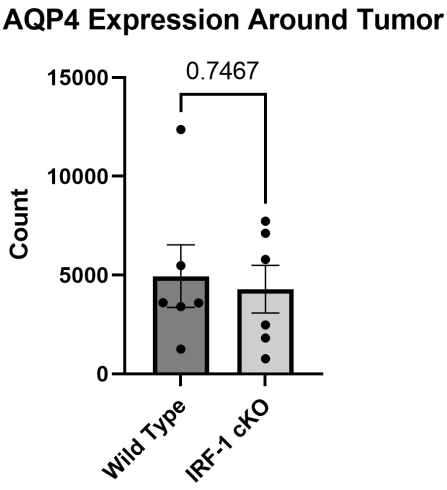

Figure 20: AQP4 Staining in the Non-Tumor Bearing Hemisphere. A) Confocal images of non-tumor bearing hemisphere sections of WT and IRF-1 cKO (20x) AQP4 (RED) and Nuclei (DAPI, BLUE) **B)** Quantification of **(A)** n=3,3, p=0.5009, T-Test

A

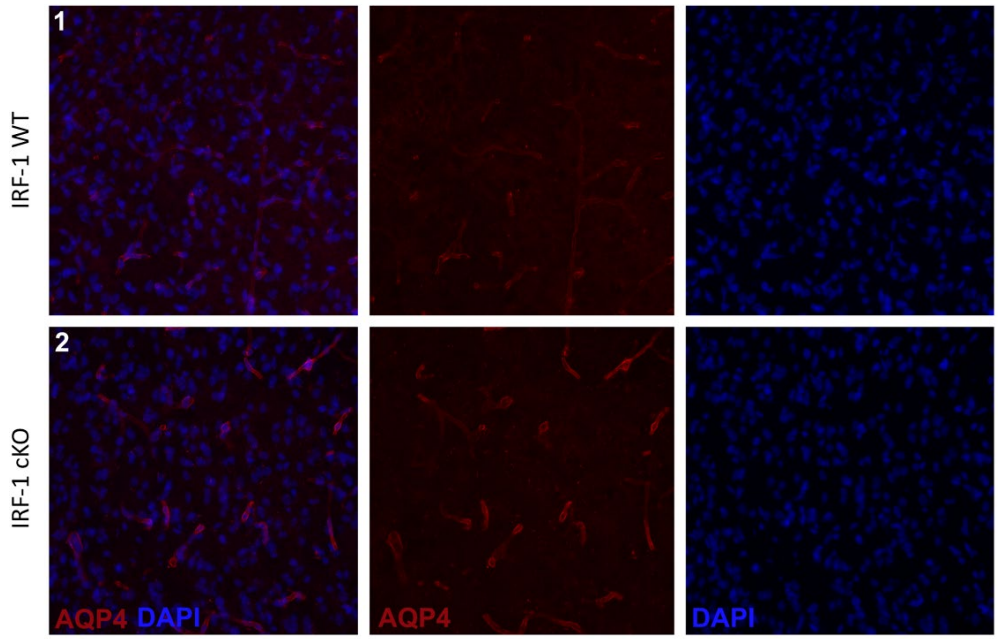

B

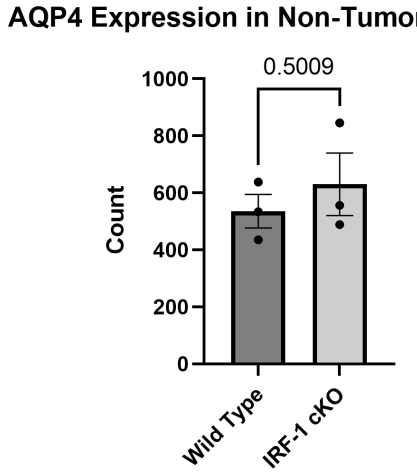

DISCUSSION

The critical role of the GBM microenvironment has been now firmly established (Zhang et al,. 2020). Although both microglia and astrocytes are known to cross-talk with GBM cells, the precise mechanisms regulating their cross-communication remain largely to be better understood. In this work, we took advantage of the new spontaneous glioma model that allows for genetic analysis of the role of genes in astrocytes and glioma cells on glioma growth and progression.

The purpose of the current work was to determine if astrocytic IRF-1 is vital for the growth and generation of spontaneous mouse gliomas. While IRF-1 prevents tumorigenesis in a spontaneous mouse model of colorectal cancer, it also controls PD-L1 expression in many cancer types (Qian et al,. 2018). These previous results led us to the hypothesis that astrocytic IRF-1 may be critical in glioma.

We employed a lentiviral-driven model of spontaneous gliomas in IRF-1 cKO mice. Surprisingly our data suggest that deletion of IRF-1 from astrocytes does not affect neither glioma generation nor mouse survival. However, our experimental setup did not allow us to examine tumor burden during the time of glioma growth. Tumor burden during glioma development may be different and thus it needs to be evaluated thus it needs to be evaluated in the future.

Our data indicate that IRF-1 regulates expression of PD-L1 in both astrocytes and glioma cells. This is a novel finding that is consistent with reports of IRF-1 dependent regulation of PD-L1 expression in other cancers (Qian et al,. 2018). However, the effect of

downregulation of PD-L1 expression in both astrocytes and glioma of IRF-1 cKO mice did not affect mice survival. These findings can be explained by abundant PD-L1 expression in myeloid cells. Our data suggests that PD-L1 in myeloid cells, that account for up to 30% of the tumor mass, may be sufficient to tone-down immune responses in glioma. This can be tested in a model of myeloid specific IRF-1 cKO mice. We would expect that immunosuppression may be removed if PD-L1 expression is abolished in myeloid cells. However, PD-L1 expression is also regulated by other mechanisms that are IRF-1-independent. In fact, PD-L1 expression is also driven by STAT3 (Qian et al,. 2018). Thus it is possible that PD-L1 can still be upregulated in myeloid cells even in the absence of IRF-1.

Importantly however, we found that PD-L1 expression is not affected in tumor-free hemispheres by the deletion of IRF-1 from astrocytes. This is expected, since IRF-1 is expressed at very low basal levels in astrocytes.

Another interesting finding is that deletion of IRF-1 from astrocytes did not affect the numbers of glioma-associated myeloid cells. This is profoundly surprising since there is excessive crosstalk between astrocytes and microglia. This data suggests that factors secreted by glioma cells are likely more important for the recruitment of myeloid cells to the tumor than factors secreted by astrocytes. Astrocytes can likely modulate this process to some extent but appear not to be critical. It remains to be established whether myeloid cell polarization is affected by IRF-1 deletion from astrocytes. This could be done by analysis of expressed cytokines as well as markers of M1 and M2 myeloid cells.

The most important finding to come from the research is that the deletion of IRF-1 from astrocytes modulated the vascularization of the tumors. Astrocytes exert their control on tumor vascularization by their endfeet interactions with endothelial cells. The data suggests that astrocytes may play a vital role in glioma vascularization and that IRF-1 is involved in this process. This finding is consistent with the previously known fact that Aquaporin-4 expression is upregulated by VEGF in tissue containing glioma (Yang et al,. 2012). Although there was no significant difference in VEGF mRNA expression, this can easily be explained by our tissue collection techniques. We used the entire tumor bearing hemisphere that was constituted of the tumor and entire normal tissue of the hemisphere. Further analysis needs to be done to analyze the tumors specifically between WT and IRF-1 cKO mice. Another key aspect that needs to be analyzed is the co-expression of CD31 and AQP4 to confirm the finding that astrocyte-specific IRF-1 influences GBM microenvironment vasculature development.

LITERATURE CITED

Hanif, F., Muzaffar, K., Perveen, K., Malhi, S. M., & Simjee, S. (2017). Glioblastoma Multiforme: A Review of its Epidemiology and Pathogenesis through Clinical Presentation and Treatment. Asian Pacific journal of cancer prevention : APJCP, 18(1), 3–9. https://doi.org/10.22034/APJCP.2017.18.1.3

Wang, X., Lu, J., Guo, G. et al. Immunotherapy for recurrent glioblastoma: practical insights and challenging prospects. Cell Death Dis 12, 299 (2021). https://doi.org/10.1038/s41419-021-03568-0

Pombo Antunes, A. R., Scheyltjens, I., Duerinck, J., Neyns, B., Movahedi, K., & Van Ginderachter, J. A. (2020). Understanding the glioblastoma immune microenvironment as basis for the development of new immunotherapeutic strategies. eLife, 9, e52176. https://doi.org/10.7554/eLife.52176

Zhang, H., Zhou, Y., Cui, B., Liu, Z., Shen, H. (2020) Novel insights into astrocyte-mediated signaling of proliferation, invasion and tumor immune microenvironment in glioblastoma, Biomedicine & Pharmacotherapy,Volume 126, 2020, https://doi.org/10.1016/j.biopha.2020.110086

Iwahori K. (2020). Cytotoxic CD8+ Lymphocytes in the Tumor Microenvironment. Advances in experimental medicine and biology, 1224, 53–62. https://doi.org/10.1007/978-3-030-35723-8_4

Schroder, K., Hertzog, P. J., Ravasi, T., & Hume, D. A. (2004). Interferon-gamma: an overview of signals, mechanisms and functions. Journal of leukocyte biology, 75(2), 163–189. https://doi.org/10.1189/jlb.0603252

Imada, K., & Leonard, W. J. (2000). The Jak-STAT pathway. Molecular immunology, 37(1-2), 1–11. https://doi.org/10.1016/s0161-5890(00)00018-3

Harrison D. A. (2012). The Jak/STAT pathway. Cold Spring Harbor perspectives in biology, 4(3), a011205. https://doi.org/10.1101/cshperspect.a011205

Qian, J., Wang, C., Wang, B. et al. The IFN-γ/PD-L1 axis between T cells and tumor microenvironment: hints for glioma anti-PD-1/PD-L1 therapy. J Neuroinflammation 15, 290 (2018). https://doi.org/10.1186/s12974-018-1330-2

Liu, J., Guan, X., Ma, X. (2005) Interferon Regulatory Factor 1 Is an Essential and Direct Transcriptional Activator for Interferon γ-induced RANTES/CCl5 Expression in Macrophages, Journal of Biological Chemistry, Volume 280, Issue 26, https://doi.org/10.1074/jbc.M500973200

Feng, H., Zhang, Y. B., Gui, J. F., Lemon, S. M., & Yamane, D. (2021). Interferon Regulatory Factor 1 (IRF1) and anti-pathogen innate immune responses. PLoS pathogens, 17(1), e1009220. https://doi.org/10.1371/journal.ppat.1009220

Harikumar, K. B., Yester, J. W., Surace, M. J., Oyeniran, C., Price, M. M., Huang, W. C., Hait, N. C., Allegood, J. C., Yamada, A., Kong, X., Lazear, H. M., Bhardwaj, R., Takabe, K., Diamond, M. S., Luo, C., Milstien, S., Spiegel, S., & Kordula, T. (2014). K63-linked polyubiquitination of transcription factor IRF1 is essential for IL-1-induced production of chemokines CXCL10 and CCL5. Nature immunology, 15(3), 231–238. https://doi.org/10.1038/ni.2810

Jarosinski, K. W., & Massa, P. T. (2002). Interferon Regulatory Factor-1 is required for interferon-gamma-induced MHC class I genes in astrocytes. Journal of neuroimmunology, 122(1-2), 74–84. https://doi.org/10.1016/s0165-5728(01)00467-2

Karki, R., Sharma, B. R., Lee, E., Banoth, B., Malireddi, R., Samir, P., Tuladhar, S., Mummareddy, H., Burton, A. R., Vogel, P., & Kanneganti, T. D. (2020). Interferon Regulatory Factor 1 regulates PANoptosis to prevent colorectal cancer. JCI insight, 5(12), e136720. https://doi.org/10.1172/jci.insight.136720

Yi, M., Niu, M., Xu, L. et al. Regulation of PD-L1 expression in the tumor microenvironment. J Hematol Oncol 14, 10 (2021). https://doi.org/10.1186/s13045-020-01027-5

Escors, D., Gato-Cañas, M., Zuazo, M., Arasanz, H., García-Granda, M. J., Vera, R., & Kochan, G. (2018). The intracellular signalosome of PD-L1 in cancer cells. Signal transduction and targeted therapy, 3, 26. https://doi.org/10.1038/s41392-018-0022-9

Ostrand-Rosenberg, S., Horn, L. A., & Haile, S. T. (2014). The programmed death-1 immune-suppressive pathway: barrier to antitumor immunity. Journal of immunology (Baltimore, Md. : 1950), 193(8), 3835–3841. https://doi.org/10.4049/jimmunol.1401572

Moon, J.W., Kong, SK., Kim, B.S. et al. IFNγ induces PD-L1 overexpression by JAK2/STAT1/IRF-1 signaling in EBV-positive gastric carcinoma. Sci Rep 7, 17810 (2017). https://doi.org/10.1038/s41598-017-18132-0

Gao, X., Li, W., Syed, F. et al. PD-L1 signaling in reactive astrocytes counteracts neuroinflammation and ameliorates neuronal damage after traumatic brain injury. J Neuroinflammation 19, 43 (2022). https://doi.org/10.1186/s12974-022-02398-x

Scheffel, T. B., Grave, N., Vargas, P., Diz, F. M., Rockenbach, L., & Morrone, F. B. (2021). Immunosuppression in Gliomas via PD-1/PD-L1 Axis and Adenosine Pathway. Frontiers in oncology, 10, 617385. https://doi.org/10.3389/fonc.2020.617385

Garcia-Diaz, A., Shin, D. S., Moreno, B. H., Saco, J., Escuin-Ordinas, H., Rodriguez, G. A., Zaretsky, J. M., Sun, L., Hugo, W., Wang, X., Parisi, G., Saus, C. P., Torrejon, D. Y., Graeber, T. G., Comin-Anduix, B., Hu-Lieskovan, S., Damoiseaux, R., Lo, R. S., & Ribas, A. (2017). Interferon Receptor Signaling Pathways Regulating PD-L1 and PD-L2 Expression. Cell reports, 19(6), 1189–1201. https://doi.org/10.1016/j.celrep.2017.04.031

Qingyang, L., Dan, W., Kai, S., Liping, W., Yi Z. (2020) Resistance Mechanisms of Anti-PD1/PDL1 Therapy in Solid Tumors. Frontiers in Cell and Developmental Biology, Volume – 8. https://www.frontiersin.org/article/10.3389/fcell.2020.00672

Yang, L., Wang, X., Zhen, S., Zhang, S., Kang, D., & Lin, Z. (2012). Aquaporin-4 upregulated expression in glioma tissue is a reaction to glioma-associated edema induced by vascular endothelial growth factor. Oncology reports, 28(5), 1633–1638. https://doi.org/10.3892/or.2012.1973

Barthel, L., Hadamitzky, M., Dammann, P. et al. Glioma: molecular signature and crossroads with tumor microenvironment. Cancer Metastasis Rev 41, 53–75 (2022). https://doi.org/10.1007/s10555-021-09997-9

Friedmann-Morvinski, D., Bushong, E. A., Ke, E., Soda, Y., Marumoto, T., Singer, O., Ellisman, M. H., & Verma, I. M. (2012). Dedifferentiation of neurons and astrocytes by oncogenes can induce gliomas in mice. *Science (New York, N.Y.)*, *338*(6110), 1080–1084. https://doi.org/10.1126/science.1226929

Henrik Heiland, D., Ravi, V.M., Behringer, S.P. et al. Tumor-associated reactive astrocytes aid the evolution of immunosuppressive environment in glioblastoma. Nat Commun 10, 2541 (2019). https://doi.org/10.1038/s41467-019-10493-6

Matias, D., Balça-Silva, J., Graça Grazielle, C., Wanjiru, C., Macharia, L., Nascimento, C., et al. (2018) Microglia/Astrocytes–Glioblastoma Crosstalk: Crucial Molecular Mechanisms and Microenvironmental Factors. *Frontiers in Cellular Neuroscience,* Volume 12. https://www.frontiersin.org/article/10.3389/fncel.2018.00235

Brandao, M., Simon, T., Critchley, G., & Giamas, G. (2019). Astrocytes, the rising stars of the glioblastoma microenvironment. Glia, 67(5), 779–790. https://doi.org/10.1002/glia.23520

Akinleye, A., Rasool, Z. Immune checkpoint inhibitors of PD-L1 as cancer therapeutics. J Hematol Oncol 12, 92 (2019). https://doi.org/10.1186/s13045-019-0779-5

Hao, C., Chen, G., Zhao, H., Li, Y., Chen, J., Zhang, H., Li, S., Zhao, Y., Chen, F., Li, W., & Jiang, W. G. (2020). PD-L1 Expression in Glioblastoma, the Clinical and Prognostic Significance: A Systematic Literature Review and Meta-Analysis. Frontiers in oncology, 10, 1015. https://doi.org/10.3389/fonc.2020.01015

Chen, R. Q., Liu, F., Qiu, X. Y., & Chen, X. Q. (2019). The Prognostic and Therapeutic Value of PD-L1 in Glioma. Frontiers in pharmacology, 9, 1503. https://doi.org/10.3389/fphar.2018.01503

Ohsugi, T., Yamaguchi, K., Zhu, C. et al. Anti-apoptotic effect by the suppression of IRF1 as a downstream of Wnt/β-catenin signaling in colorectal cancer cells. Oncogene 38, 6051–6064 (2019). https://doi.org/10.1038/s41388-019-0856-9

Thomas, S., Snowden, J., Zeidler, M. et al. The role of JAK/STAT signalling in the pathogenesis, prognosis and treatment of solid tumours. Br J Cancer 113, 365–371 (2015). https://doi.org/10.1038/bjc.2015.233

VITA

Aakash Vaidya was born in Mumbai, India on January 1st, 1996. He has lived in a multitude of places after immigrating to America including Alabama, Colorado, and currently, Virginia. He completed his undergraduate at the University of Colorado Boulder where he got his Bachelor of Sciences in Finance and Marketing. Following graduation, he worked a while in corporate before shifting his focus to the sciences. He completed the Health Sciences Certificate program at Virginia Commonwealth University to strengthen his application to medical school. After taking a year to prepare for the MCAT while navigating the Covid pandemic landscape, he applied for the Biochemistry Master's program at Virginia Commonwealth University. Upon graduation he is expected to continue his education at Liberty University College of Osteopathic Medicine to further pursue his goal of becoming a physician. He hopes to use his varying background to give the best patient centered care that he is capable of delivering.